

Loops in inflation with strongly non-geodesic motion

Sebastian Garcia-Saenz,^a Yizhou Lu,^{a,b,c} Sébastien Renaux-Petel^d

^aDepartment of Physics, Southern University of Science and Technology, Shenzhen 518055, China

^bShanghai Institute for Mathematics and Interdisciplinary Sciences, Shanghai 200000, China

^cSchool of Mathematical Sciences, Fudan University, Shanghai 200000, China

^dInstitut d'Astrophysique de Paris, UMR 7095 du CNRS et de Sorbonne Université, 98 bis Boulevard Arago, 75014 Paris, France

E-mail: sgarciasaenz@sustech.edu.cn, luyz@simis.cn, renaux@iap.fr

Abstract. We study loop corrections in the effective field theory of inflation with imaginary speed of sound, which has been shown to provide an effective description of multi-field inflationary models characterized by strongly non-geodesic motion and heavy entropic perturbations. We focus on the one-loop corrections to the scalar and tensor power spectra, taking into account all relevant vertices at leading order in derivatives and in slow-roll. We find a power-law dependence of the scalar two-point function on the scale that defines the range of validity of the effective theory, analogous to the enhancement observed in tree-level correlation functions. Even more dramatic, the relative correction to the tensor spectrum is exponentially enhanced, albeit also suppressed in the slow-roll limit. In spite of these large effects, our results show that this class of models can satisfy the requirement of perturbative control and a consistent loop expansion within a range of parameters of phenomenological interest. On the other hand, models predicting large values of the power spectrum on small scales are found to be under strong tension. As a technical bonus, we carefully explain the prescription for the regularization and manipulation of loop integrals in this set-up, where one has a non-trivial domain of integration for time and momentum integrals owing to the regime of validity of the effective field theory. This procedure is general enough to be of potential applicability in other contexts.

Contents

1	Introduction	1
2	EFT with imaginary speed of sound and loop integrals	4
2.1	Quadratic action and quantization	4
2.2	Interaction vertices	8
2.3	In-in formalism	9
2.4	Cutting off loop integrals	9
2.4.1	Loop with one quartic vertex	10
2.4.2	Loop with two cubic vertices	10
3	One-loop scalar power spectrum	14
3.1	Loops with two cubic vertices	14
3.2	Loops with one quartic vertex	17
3.3	Counterterms and higher derivative corrections	18
4	One-loop tensor power spectrum	20
4.1	Loops with two cubic vertices	20
4.2	Loops with one quartic vertex	22
5	Discussion	24
A	Lowest-order EFT and k-inflation	25
B	Scalar loop from $H_{\zeta\zeta\zeta}^{(2)}$	26
C	Other quartic scalar vertices	28

1 Introduction

Scalar and tensor inhomogeneities on small scales — i.e. wavelengths shorter than those probed in the cosmic microwave background (CMB) and large-scale structure surveys — are a primary target of current and future cosmological experiments. A positive detection could potentially provide invaluable information about the physics of the dark era of inflation following the horizon crossing of CMB-scale fluctuations, i.e. a large number of e-folds of evolution about which we have essentially no experimental knowledge so far.

There is no good reason to expect the near-perfect scale invariance of perturbations observed in the CMB to extrapolate until the end of inflation. Transient violations of slow-roll, triggered for instance by features in the scalar potential, see e.g. [1–27], may enhance scalar inhomogeneities to observable levels, for example through their effect on primordial black hole formation [28–30]. Moreover, scalar fluctuations also source tensor modes, i.e. induced gravitational waves (GWs) [31–35], which could be directly detected by next-generation experiments and might have in fact already been discovered in pulsar timing array data [36–44]. Even on CMB scales, actually, departures from the ‘vanilla’-type scenario of single-field slow-roll inflation are of course also interesting even if already constrained by observations. This is particularly relevant in relation to the higher-point statistics of the perturbations, i.e. the

non-Gaussianities, which encode information on the microscopic physics of inflation and its particle content [45–49]. There is therefore a strong motivation to thoroughly understand, on the theoretical side, the physical mechanisms that could give rise to a magnification of scalar perturbations and to large non-Gaussianities. Multi-field inflation provides a natural arena to investigate this question in view of the wealth of possible interesting dynamics that would not be available in the case of a single degree of freedom. Two uniquely multi-field features that are worth highlighting are the (generic) presence of a curved field space, i.e. a non-linear sigma model where the kinetic term of the scalar fields ϕ^I has the form $G_{IJ}(\phi)\nabla^\mu\phi^I\nabla_\mu\phi^J$ with non-flat ‘internal’ metric G_{IJ} , and the possibility that the inflaton trajectory may deviate from a geodesic in the space spanned by the fields ϕ^I .

In fact, in negatively curved field spaces, slow-roll trajectories tend to be geometrically destabilized, in which case the inflationary fields bifurcate into another attractor regime characterized by a strongly non-geodesic motion [50]. This mechanism to inflate is radically different from slow-roll, it naturally predicts large non-Gaussianities and it has been extensively studied in the past few years, see e.g. [50–78]. Considering for concreteness an adiabatic-entropic decomposition of the scalar fields’ perturbations [79] and assuming the well-motivated scenario in which the entropic modes are heavy (in a sense to be made more precise below), one is led to an effective single-field description in which the adiabatic mode propagates with sub-luminal speed of sound given by [80, 81]

$$\frac{1}{c_s^2} = 1 + \frac{4H^2\eta_\perp^2}{m_s^2}, \quad (1.1)$$

where H is the Hubble scale, η_\perp is a dimensionless parameter that quantifies the degree of geodesic deviation and m_s^2 is a scale related to the effective mass of the entropic perturbations (see e.g. Ref. [63] for the precise definitions and further details). Note that all these quantities are in general time-dependent, although in this paper we will assume throughout adiabaticity conditions [82, 83] and thus approximate them as constants. By definition, we speak of a strongly non-geodesic field trajectory as one with large bending parameter, $|\eta_\perp| \gg 1$. More precisely, for reasons we explain below, in this paper we will be interested in a regime where $\eta_\perp^2 \gtrsim m_s^2/H^2 \gg 1$. This condition implies that c_s^2 , when positive, must be parametrically smaller than unity. As is well known, this scenario of reduced speed of sound leads to large non-Gaussianities as one of its key predictions [84, 85].

In slow-roll and slow-turn inflation, i.e. with $|\eta_\perp| \lesssim 1$, the entropic mass squared, m_s^2 , is always a positive quantity. However, m_s^2 is a derived parameter, unrelated to the mass of any fundamental particle, and in general it can have either sign. Explicitly, in non-linear sigma models with two fields, one has

$$m_s^2 = V_{;ss} - H^2\eta_\perp^2 + \epsilon H^2 M_{\text{Pl}}^2 R_{\text{fs}}, \quad (1.2)$$

where $V_{;ss}$ is the second field space-covariant derivative of the potential projected along the entropic direction, M_{Pl} is the Planck mass and R_{fs} is the curvature scalar of the internal space. The latter of course need not be positive, and in fact negatively curved field spaces are especially well-motivated by constructions of inflationary models within supergravity [50, 55, 86, 87]. More to the point, the bending parameter always gives a negative contribution to m_s^2 , and indeed several explicit models are characterized by background solutions with $m_s^2 < 0$, see e.g. [50, 56, 58, 64]. Beyond two fields, the entropic mass (in general a matrix) also includes terms related to the ‘twist’ of the adiabatic-entropic basis, and these too will typically give negative contributions [68, 72, 76, 88, 89].

Even though m_s^2 does not properly correspond to any mass eigenstate, the intuition that a negative squared mass is associated to a tachyonic instability may be shown to be correct. Explicit computations indeed indicate, in this class of set-ups, that perturbations experience an exponential enhancement starting around the time of ‘mass-shell’ crossing, $k^2/a^2 \sim |m_s^2|$ [58, 59]. At earlier times, i.e. for larger physical momenta, the instability is absent, as expected of tachyonic modes. Unlike for tachyonic fields in flat spacetime, however, the instability is also quenched soon after horizon crossing. This is so because, in the super-Hubble regime, entropic fluctuations evolve independently of adiabatic ones, and a good notion of effective mass may be defined in this context. This mass is however different from m_s^2 ; specifically in two-field models it is given by $m_{s,\text{eff}}^2 = m_s^2 + 4H^2\eta_\perp^2$. We see therefore that a large bending has the ability to both trigger a transient tachyonic destabilization while at the same time to render the super-horizon fluctuations (and hence the background in particular) stable. In fact, since typically one has $m_{s,\text{eff}}^2 \gg H^2$ in scenarios with strongly non-geodesic motion, entropic modes quickly decay after horizon crossing and the curvature perturbation reaches an adiabatic limit.

A tachyonic instability during inflation leads to several interesting observational signatures. At the level of the two-point function, the exponential enhancement of scalar fluctuations translates into a very small tensor-to-scalar ratio, so that a detection of tensor modes in the CMB could easily falsify this scenario. More promising and intriguing however is the possibility of probing inflationary tachyonic modes through higher-point statistics. Non-Gaussianities in this context have been shown to be large, as in reduced speed of sound scenarios, but with distinctive shapes: the bispectrum overlaps strongly with the orthogonal template [59], while higher-point correlators are similarly enhanced on ‘flattened’ polygon configurations [64, 67].

Although a tachyonic instability in inflation is necessarily transient, as we have explained, the exponential growth still carries the risk of impairing the perturbative description. This question motivates us to tackle the problem of assessing the size of loop corrections in models with tachyonic modes. Concretely, we want to see under what conditions the one-loop corrections to the scalar power spectrum is smaller than the tree-level result. Here ‘loops’ are understood in the sense of the in-in formalism [90] and hence include both classical and quantum effects.

We are also interested in assessing the size of scalar loop corrections to the tensor power spectrum. In this case, a large one-loop contribution need not be associated with the breakdown of perturbativity, since one may still a priori have a consistent expansion for the higher-order loops. This could result in a significant contribution to scalar-induced GWs during inflation [21, 91–94]. In this event, a tachyonic instability could serve as a mechanism to enhance tensor fluctuations to levels of interest for current and future GW detectors. Beyond this interesting phenomenological aspect, and more to the point of this paper, the tensor spectrum is also another observable that may be used for diagnosing the perturbativity of the theory.

Having established these goals, one is faced with the technically challenging task of calculating loop integrals in complex multi-field models in which the mode functions are not known analytically. In this paper we bypass this issue by resorting to the effective field theory (EFT) of single-field inflation [85], assuming further the limits of slow-roll and adiabaticity. Besides the fact that this approach will allow us to obtain fully analytical expressions (with some approximations and assumptions to be made explicit below), it has the added advantage that it provides results that are universal, within its regime of validity, as is usual with EFT.

The EFT of inflation derived from integrating out a tachyonic ($m_s^2 < 0$) and heavy ($|m_s^2| \gg H^2$) mode was introduced in [58] and further studied in [59, 64, 71, 95] (see also [51] for an earlier work). The structure of the theory is equivalent to that of the standard EFT of [85], the only peculiarity being that the squared speed of sound, c_s^2 , of the adiabatic fluctuation is negative in this set-up, hence the so-called scenario of imaginary speed of sound. If c_s is imaginary, the mode function is not oscillatory but exponentially growing or decaying, which is nothing but a manifestation of the tachyonic instability of the multi-field theory. Although the instability in the EFT may seem more drastic (a wrong-sign gradient term versus a wrong-sign mass term in the case of a tachyon), one must remember that any EFT is self-consistently endowed with an energy cutoff, which in the present context naturally limits the regime of validity of the theory to capture the physics around the time of sound horizon crossing. In this regime, then, a breakdown of perturbativity in the multi-field theory should imply an equivalent breakdown in the single-field EFT. Remarkably, at *tree level*, n -point correlation functions of the adiabatic fluctuation have been shown to admit a consistent perturbative expansion [64]. As explained, one of our goals here is to address this question at the one-loop level.

Sec. 2 contains all the background material we will make use of in our calculations, including a brief review of the EFT of inflation with imaginary sound speed, of the in-in formalism, and a discussion on the manipulation of the loop integrals in the presence of an explicit momentum cutoff. To our knowledge this last aspect has not been addressed previously in the literature, which we think may prove useful in other contexts. Sec. 3 presents our calculation of the one-loop correction to the scalar power spectrum. Our results are fully analytic although not exhaustive, as we consider the approximation of large x (the dimensionless parameter defining the momentum cutoff of the EFT, to be defined explicitly below) and moreover we do not calculate all the possible diagrams. Nevertheless, we also provide a scaling argument which shows that the neglected diagrams must yield similar results and would therefore not modify our final estimates. The same calculation for the tensor power spectrum is given in Sec. 4, using the same large- x approximation. The conclusions that follow from our results, together with an outlook of our paper, are discussed in Sec. 5. Some technical aspects and details of our calculations are relegated to the appendices.

2 EFT with imaginary speed of sound and loop integrals

2.1 Quadratic action and quantization

The construction of the EFT of inflation with imaginary speed of sound is equivalent to that of the standard set-up [85] (see also [96] for a review). Throughout this paper we focus exclusively on the EFT at lowest order in the derivative expansion and leading order in the slow-roll approximation. This set-up is thus equivalent to the theory of k-inflation [97, 98] at lowest order in the slow-roll expansion; see Appendix A for details.

At quadratic order in perturbations one has the Lagrangian

$$S_2 = \int d\eta d^3\mathbf{x} a^2 \left[\frac{\epsilon M_{\text{Pl}}^2}{c_s^2} (\zeta'^2 - c_s^2 (\partial\zeta)^2) + \frac{M_{\text{Pl}}^2}{8} (\gamma'_{ij}\gamma'_{ij} - \partial_k\gamma_{ij}\partial_k\gamma_{ij}) \right], \quad (2.1)$$

for the adiabatic curvature perturbation ζ and the transverse and traceless metric perturbation γ_{ij} . Here $a(\eta)$ is the scale factor defined in terms of conformal time η , and primes denote derivatives with respect to η . M_{Pl} , ϵ and c_s^2 are respectively the Planck mass, first slow-roll

parameter and squared speed of sound. Both ϵ and c_s^2 are assumed constant at the order we work on in the slow-roll approximation, and consistently with this we have $a(\eta) = -1/(H\eta)$, with H the Hubble parameter.

As explained in the Introduction, c_s^2 is a derived quantity related to parameters of the multi-field theory, and may actually be negative. This is the scenario we consider in this paper, and from now on we write $c_s^2 = -|c_s|^2$ to be explicit. From (2.1) we infer that ζ is then a ghost field (wrong-sign kinetic term) and gradient-unstable (exponentially growing solutions). Nevertheless, keeping in mind that this is an EFT with a limited regime of validity (to be discussed below), nothing prevents one from carrying out the canonical quantization as usual. This was done in [59] and we review this procedure next.

Promoting ζ to a quantum field, it is decomposed in Fourier modes as

$$\hat{\zeta}(\eta, \mathbf{x}) = \int \frac{d^3\mathbf{k}}{(2\pi)^3} \hat{\zeta}_{\mathbf{k}}(\eta) e^{i\mathbf{k}\cdot\mathbf{x}}, \quad (2.2)$$

with

$$\hat{\zeta}_{\mathbf{k}} = \zeta_k(\eta) a_{\mathbf{k}} + \zeta_k^*(\eta) a_{-\mathbf{k}}^\dagger, \quad (2.3)$$

in terms of the mode function $\zeta_k(\eta)$ and the annihilation and creation operators \hat{a} and \hat{a}^\dagger . The latter satisfy the commutation relations

$$[\hat{a}_{\mathbf{k}}, \hat{a}_{\mathbf{p}}^\dagger] = (2\pi)^3 \delta^3(\mathbf{k} - \mathbf{p}), \quad [\hat{a}_{\mathbf{k}}, \hat{a}_{\mathbf{p}}] = [\hat{a}_{\mathbf{k}}^\dagger, \hat{a}_{\mathbf{p}}^\dagger] = 0. \quad (2.4)$$

The free-theory equation of motion for ζ_k that follows from (2.1) reads

$$\zeta_k'' - \frac{2}{\eta} \zeta_k' - |c_s|^2 k^2 \zeta_k = 0, \quad (2.5)$$

with general solution

$$\zeta_k(\eta) = \zeta_{k,+}(\eta) + \zeta_{k,-}(\eta), \quad (2.6)$$

and we introduce what we call the growing and decaying modes, respectively given by

$$\zeta_{k,+} \equiv \frac{A_k}{k^{3/2}} e^{k|c_s|\eta} (k|c_s|\eta - 1), \quad \zeta_{k,-} \equiv -\frac{B_k}{k^{3/2}} e^{-k|c_s|\eta} (k|c_s|\eta + 1). \quad (2.7)$$

Here A_k and B_k are integration constants, a priori dependent on k ; the reason for extracting the factors of $k^{3/2}$ will become clear in a moment.

Let $\mathcal{P}_\zeta(\eta, \mathbf{x}) \equiv \partial\mathcal{L}_2/\partial\zeta'$ be the canonical momentum. The quantization condition $[\hat{\zeta}(\eta, \mathbf{x}), \hat{\mathcal{P}}_\zeta(\eta, \mathbf{y})] = i\delta^3(\mathbf{x} - \mathbf{y})$ then translates into

$$\zeta_k \zeta_k^{*'} - \zeta_k' \zeta_k^* = -\frac{i|c_s|^2}{2\epsilon a^2 M_{\text{Pl}}^2}, \quad (2.8)$$

or equivalently

$$\text{Im}[A_k^* B_k] = \frac{H^2}{8|c_s| M_{\text{Pl}}^2 \epsilon}. \quad (2.9)$$

This last relation shows that both the growing and decaying modes must be present, unlike what occurs in the standard set-up with real c_s , where one typically chooses one solution corresponding to the Bunch-Davies vacuum.

2.2 Interaction vertices

The one-loop scalar and tensor spectra receive contributions from diagrams involving the cubic and quartic couplings of the theory. Recall that we focus on the slow-roll approximation, however as we are interested in couplings mixing the adiabatic mode with gravity, we do not strictly take the so-called decoupling limit, but instead keep the leading-order vertices of each type. At cubic order we consider

$$S_3 = - \int d\eta d^3\mathbf{x} a \frac{M_{\text{Pl}}^2 \epsilon}{H |c_s|^2} (1 + |c_s|^2) \left[- \frac{\mathcal{A}}{|c_s|^2} \zeta'^3 + \zeta' (\partial\zeta)^2 \right] - \int d\eta d^3\mathbf{x} a^2 \epsilon M_{\text{Pl}}^2 \gamma_{ij} \partial_i \zeta \partial_j \zeta. \quad (2.26)$$

Here the first terms correspond to the $\zeta\zeta\zeta$ vertices appearing in the EFT of inflation at leading order in the slow-roll approximation, with \mathcal{A} a dimensionless constant. Similarly, the second term is the leading-order $\gamma\zeta\zeta$ vertex, corresponding to the universal minimal gravitational coupling. As already mentioned, this action also coincides with the cubic-order expansion of k-inflation [45, 84] (see Appendix A for details). For later use we list here the interaction Hamiltonians for the individual vertices:³

$$H_{\zeta\zeta\zeta}^{(1)}(\eta) = \mathcal{C} a \int d^3\mathbf{x} \zeta'^3, \quad \mathcal{C} \equiv - \frac{M_{\text{Pl}}^2 \epsilon}{H} \left(1 + \frac{1}{|c_s|^2} \right) \frac{\mathcal{A}}{|c_s|^2}, \quad (2.27)$$

$$H_{\zeta\zeta\zeta}^{(2)}(\eta) = \tilde{\mathcal{C}} a \int d^3\mathbf{x} \zeta' (\partial\zeta)^2, \quad \tilde{\mathcal{C}} \equiv \frac{M_{\text{Pl}}^2 \epsilon}{H} \left(1 + \frac{1}{|c_s|^2} \right), \quad (2.28)$$

$$H_{\gamma\zeta\zeta}(\eta) = \mathcal{E} a^2 \int d^3\mathbf{x} \gamma_{ij} \partial_i \zeta \partial_j \zeta, \quad \mathcal{E} \equiv M_{\text{Pl}}^2 \epsilon. \quad (2.29)$$

At quartic order in perturbations, and always at leading order in slow-roll, the EFT of inflation contains three $\zeta\zeta\zeta\zeta$ vertices. For simplicity, and in line with our aim of estimating the size of loop corrections rather than calculating exact values, we focus here on a single vertex, namely ζ'^4 . We do not expect the other two vertices to give qualitatively different results, and indeed we argue in Appendix C that the one-loop scalar power spectrum for all three vertices should have the same scaling with x in the large- x limit, which we moreover confirm through an explicit calculation with the $(\partial\zeta)^4$ vertex. In addition, we have two mixed quartic couplings $\gamma\gamma\zeta\zeta$ at leading order in derivatives and slow-roll, leading to the following set of interaction Hamiltonians:

$$H_{\zeta\zeta\zeta\zeta}^{(1)}(\eta) = \mathcal{D} \int d^3\mathbf{x} \zeta'^4, \quad \mathcal{D} \equiv \frac{M_{\text{Pl}}^2 \epsilon}{H^2 |c_s|^6} \mathcal{D}, \quad (2.30)$$

$$H_{\gamma\gamma\zeta\zeta}^{(1)}(\eta) = \mathcal{F} a^2 \int d^3\mathbf{x} \gamma_{ij}^2 \zeta'^2, \quad \mathcal{F} \equiv \frac{M_{\text{Pl}}^2 \epsilon}{|c_s|^2} \mathcal{F}, \quad (2.31)$$

$$H_{\gamma\gamma\zeta\zeta}^{(2)}(\eta) = \tilde{\mathcal{F}} a^2 \int d^3\mathbf{x} \gamma_{ij}^2 (\partial\zeta)^2, \quad \tilde{\mathcal{F}} \equiv M_{\text{Pl}}^2 \epsilon \tilde{\mathcal{F}}. \quad (2.32)$$

Here \mathcal{D} , \mathcal{F} and $\tilde{\mathcal{F}}$ are some dimensionless constants, generically of $\mathcal{O}(1)$ in the EFT context.⁴ In principle they could be computed explicitly in terms of Wilson coefficients appearing in

³We define the Hamiltonian with respect to conformal time η .

⁴More in detail, we expect \mathcal{D} , \mathcal{F} and $\tilde{\mathcal{F}}$ to be combinations of $|c_s|^2$ and order-one constants, see e.g. [99] for \mathcal{D} . Barring fine tuning, they are therefore $\mathcal{O}(1)$ if $|c_s| \lesssim 1$, but not if $|c_s| \gg 1$ (see footnote 8 in relation to this point). This minor caveat is anyway unimportant for us, since we will see that the quartic vertices only play a minor role in our main results.

the EFT Lagrangian, however we have not carried out this cumbersome calculation, since anyway we are not interested in $\mathcal{O}(1)$ numbers. Notice incidentally that the last term, $H_{\gamma\zeta\zeta}^{(2)}$, is nothing but the universal contribution from the minimal gravitational coupling.

2.3 In-in formalism

We employ the standard in-in formalism [90] in our computations (see e.g. [45, 47] for reviews). The master formula giving the vacuum expectation value of an operator \hat{Q} is

$$\langle\hat{Q}(\eta)\rangle = \langle 0|U_{\text{int}}^\dagger(\eta, \eta_0)\hat{Q}_I(\eta)U_{\text{int}}(\eta, \eta_0)|0\rangle, \quad (2.33)$$

where $|0\rangle$ is the vacuum of the free theory, the subscript on \hat{Q}_I means that this is an interaction-picture operator, and

$$U_{\text{int}}(\eta, \eta_0) = T \exp \left[-i \int_{\eta_0}^{\eta} d\tilde{\eta} \hat{H}_{\text{int}}(\tilde{\eta}) \right], \quad (2.34)$$

with T the time-ordering operator and \hat{H}_{int} the interaction Hamiltonian (expressed in the interaction picture).

We are interested in the one-loop contribution to the two-point correlation function of ζ (or γ_{ij}). The master formula in this case yields two terms, corresponding to two classes of diagrams: one with two insertions of the cubic-order Hamiltonian, \hat{H}_3 ,

$$\begin{aligned} \langle\hat{\zeta}_{\mathbf{k}}(\eta)\hat{\zeta}_{\mathbf{p}}(\eta)\rangle^{(1\text{-loop})} &= 2 \text{Re} \left[\int_{\eta_0}^{\eta} d\eta_1 \int_{\eta_0}^{\eta_1} d\eta_2 \langle 0|\hat{H}_3(\eta_1)\hat{\zeta}_{\mathbf{k}}(\eta)\hat{\zeta}_{\mathbf{p}}(\eta)\hat{H}_3(\eta_2) \right. \\ &\quad \left. - \hat{\zeta}_{\mathbf{k}}(\eta)\hat{\zeta}_{\mathbf{p}}(\eta)\hat{H}_3(\eta_1)\hat{H}_3(\eta_2)|0\rangle \right], \end{aligned} \quad (2.35)$$

and one with one insertion of the quartic-order Hamiltonian, \hat{H}_4 ,

$$\langle\hat{\zeta}_{\mathbf{k}}(\eta)\hat{\zeta}_{\mathbf{p}}(\eta)\rangle^{(1\text{-loop})} = -2 \text{Im} \left[\int_{\eta_0}^{\eta} d\eta_1 \langle 0|\hat{H}_4(\eta_1)\hat{\zeta}_{\mathbf{k}}(\eta)\hat{\zeta}_{\mathbf{p}}(\eta)|0\rangle \right]. \quad (2.36)$$

In order to lighten the notation, we will omit from now on the label ‘1-loop’ and the hats in correlators. Using the usual notation where a prime on a correlator means that a factor of $(2\pi)^3$ and a momentum-conserving delta function have been stripped, we will moreover also frequently omit the labels indicating the external momenta \mathbf{k} and \mathbf{p} and external time η , i.e.

$$\langle\hat{\zeta}_{\mathbf{k}}(\eta)\hat{\zeta}_{\mathbf{p}}(\eta)\rangle^{(1\text{-loop})} \equiv (2\pi)^3 \delta(\mathbf{k} + \mathbf{p}) \langle\zeta^2\rangle', \quad (2.37)$$

and we will quote results for the function $\langle\zeta^2\rangle'$ thus defined, or rather the dimensionless combination $\frac{k^3}{2\pi^2} \langle\zeta^2\rangle'$.

2.4 Cutting off loop integrals

Eqs. (2.35) and (2.36) are defined in terms of a reference initial time η_0 . In standard set-ups with Bunch-Davies initial conditions, one is instructed to take $\eta_0 \rightarrow -\infty$ (with an appropriate $i\epsilon$ prescription to ensure convergence) in order to correctly capture all contributions to the correlators. In models with imaginary speed of sound, on the other hand, one is dealing with an EFT with a finite range of validity: the theory is valid only after a time such that all modes have energies below the cutoff scale $\Lambda \equiv xH$, where x is the parameter already introduced

in Sec. 2.1. Given a comoving momentum p and time η , this cutoff then translates into the inequality

$$-p|c_s|\eta \leq x, \quad (2.38)$$

as a restriction on each mode for it to be in the regime of validity of the EFT. For tree-level computations, this implies that the time integrals in the in-in master formula are cut off by the time $\eta_0 = -x/(k|c_s|)$, where k is the largest among all external momenta. Additional care is needed with loop diagrams, since now one also must take into account the internal momenta running in the loops, as we discuss in detail next. Notice incidentally that (2.38) is consistent with the regularization prescription discussed in [100], which emphasized the importance of setting a cutoff for *physical* momenta, i.e. $p/a(\eta) \propto p\eta$, rather than for comoving momenta.

2.4.1 Loop with one quartic vertex

We start by scrutinizing (2.36), which is the simplest case. The quartic Hamiltonian is first expressed in Fourier space, for example

$$H_{\zeta\zeta\zeta\zeta}^{(1)} = \mathcal{D}(2\pi)^3 \prod_{i=1}^4 \int \frac{d^3\mathbf{p}_i}{(2\pi)^3} \delta\left(\sum_{j=1}^4 \mathbf{p}_j\right) \zeta'_{\mathbf{p}_1} \zeta'_{\mathbf{p}_2} \zeta'_{\mathbf{p}_3} \zeta'_{\mathbf{p}_4}, \quad (2.39)$$

so that, after using all delta functions (except for the one enforcing external momentum conservation), one is left with a single, one-dimensional momentum integral, i.e. the magnitude of the loop momentum (let us call it p_1), in addition to the time integral (let us call the integration variable η_1). All in all the loop contains four physical momenta (here k is the external comoving momentum and η is the external time): $k/a(\eta)$, $k/a(\eta_1)$, $p_1/a(\eta)$ and $p_1/a(\eta_1)$. These must all satisfy the bound (2.38), i.e. $-k|c_s|\eta \leq x$, $-k|c_s|\eta_1 \leq x$, $-p_1|c_s|\eta \leq x$ and $-p_1|c_s|\eta_1 \leq x$. The first and third of these are redundant since $\eta_1 \leq \eta$; the second sets a lower limit on the time integral, while the last condition sets an upper limit on the momentum integral, that is

$$\int_{\eta_0}^{\eta} d\eta_1 \int_0^{\infty} dp_1 \quad \rightarrow \quad \int_{-x/(k|c_s|)}^{\eta} d\eta_1 \int_0^{-x/(\eta_1|c_s|)} dp_1. \quad (2.40)$$

Since the remaining integral is manifestly convergent (the integrand does not contain any singularities), we are allowed to exchange the order of integration, which is often convenient both for analytical and numerical calculations. In this case the bound $-p_1|c_s|\eta \leq x$ sets the upper limit of the momentum integral,

$$\int_{-x/(k|c_s|)}^{\eta} d\eta_1 \int_0^{-x/(\eta_1|c_s|)} dp_1 = \int_0^{-x/(|c_s|\eta)} dp_1 \int_{\eta_0}^{\eta} d\eta_1, \quad (2.41)$$

with $\eta_0 = \max\{-x/(k|c_s|), -x/(p_1|c_s|)\}$.

2.4.2 Loop with two cubic vertices

The loop integral in (2.35) contains two time integrations and a two-dimensional momentum integration, again after exploiting all available delta functions. A useful recasting of the

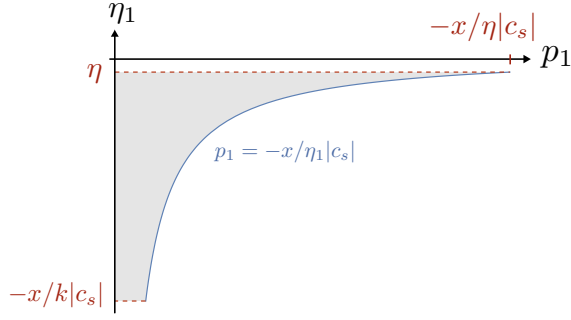


Figure 1. The integration domain in the loop diagram with one quartic vertex.

momentum integrals is given by⁵

$$\int_{\eta_0}^{\eta} d\eta_1 \int_{\eta_0}^{\eta_1} d\eta_2 \int_0^{\infty} dp_1 \int_{|k-p_1|}^{k+p_1} dp_2. \quad (2.42)$$

This integral must be cut off according to the prescription (2.38). The loop diagram contains a total of seven physical momenta, giving a total of seven constraints:

$$\begin{aligned} -q_i |c_s| \eta_j \leq x, \quad q_i \in \{k, p_1, p_2\}, \quad \eta_j \in \{\eta_1, \eta_2\}, \\ \text{and} \quad -k |c_s| \eta \leq x. \end{aligned} \quad (2.43)$$

In particular, since $\eta_2 < \eta_1$, we have $p_{1,2} \in (0, -x/|c_s|\eta_2)$. We may then identify two cases depending on the value of η_2 .

- If $k < -x/(|c_s|\eta_2) < 2k \Leftrightarrow -x/(k|c_s|) < \eta_2 < -x/(2k|c_s|)$, the integral may be divided into the following three parts:

$$\begin{aligned} \left(\int dp_1 \int dp_2 \right)_1 \equiv & \int_0^{-x/(|c_s|\eta_2)-k} dp_1 \int_{k-p_1}^{k+p_1} dp_2 + \int_{-x/(|c_s|\eta_2)-k}^k dp_1 \int_{k-p_1}^{-x/(|c_s|\eta_2)} dp_2 \\ & + \int_k^{-x/(|c_s|\eta_2)} dp_1 \int_{p_1-k}^{-x/(|c_s|\eta_2)} dp_2; \end{aligned} \quad (2.44)$$

- If $-x/(|c_s|\eta_2) > 2k \Leftrightarrow \eta_2 > -x/(2k|c_s|)$, the integral may be divided into the following three parts:

$$\begin{aligned} \left(\int dp_1 \int dp_2 \right)_2 \equiv & \int_0^k dp_1 \int_{k-p_1}^{k+p_1} dp_2 + \int_k^{-x/(|c_s|\eta_2)-k} dp_1 \int_{p_1-k}^{p_1+k} dp_2 \\ & + \int_{-x/(|c_s|\eta_2)-k}^{-x/(|c_s|\eta_2)} dp_1 \int_{p_1-k}^{-x/(|c_s|\eta_2)} dp_2. \end{aligned} \quad (2.45)$$

⁵To obtain this starting with the 6-dimensional momentum integral, one uses the identity

$$k \int d^3 \mathbf{p}_1 \int d^3 \mathbf{p}_2 \delta^3(\mathbf{p}_1 + \mathbf{p}_2 + \mathbf{k}) f(p_1, p_2, k) = 2\pi \int_0^{\infty} dp_1 \int_{|p_1-k|}^{p_1+k} dp_2 p_1 p_2 f(p_1, p_2, k).$$

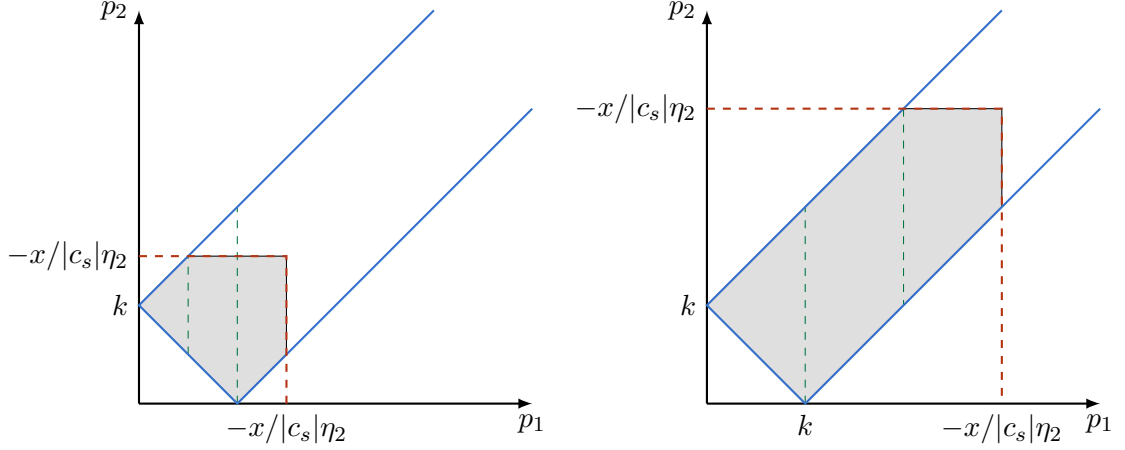


Figure 2. The integration domain for the momentum integrals in the loop diagram with two cubic vertices. The gray region corresponds to the domain after introducing the EFT cutoff, which may be divided into three parts (indicated by the green dashed lines) for the purpose of calculating the integrals. The two graphs show the two qualitatively distinct cases arising from this division.

The two cases are illustrated in Fig. 2. Since η_2 is bounded by η_1 , we further decompose the η_1 integral as follows:

$$\int_{-x/(k|c_s|)}^{\eta} d\eta_1 \equiv \left(\int d\eta_1 \right)_1 + \left(\int d\eta_1 \right)_2, \quad (2.46)$$

with

$$\left(\int d\eta_1 \right)_1 \equiv \int_{-x/(k|c_s|)}^{-x/(2k|c_s|)} d\eta_1, \quad \left(\int d\eta_1 \right)_2 \equiv \int_{-x/(2k|c_s|)}^{\eta} d\eta_1. \quad (2.47)$$

We have assumed that the external time, η , is late enough so that $\eta > -x/(2k|c_s|)$. If $-x/(k|c_s|) < \eta_1 < -x/(2k|c_s|)$, then we do not need to split the η_2 -integral and we simply write

$$\int_{-x/k|c_s|}^{\eta_1} d\eta_2 \equiv \left(\int d\eta_2 \right)_1, \quad (2.48)$$

and the corresponding momentum integrals in this case are given by $(\int dp_1 dp_2)_1$. If, on the other hand, $-x/(2k|c_s|) < \eta_1 < \eta$ then we separate the integral as

$$\int_{-x/(k|c_s|)}^{\eta_1} d\eta_2 \equiv \left(\int d\eta_2 \right)_2 + \left(\int d\eta_2 \right)_3, \quad (2.49)$$

with

$$\left(\int d\eta_2 \right)_2 \equiv \int_{-x/(k|c_s|)}^{-x/(2k|c_s|)} d\eta_2, \quad \left(\int d\eta_2 \right)_3 \equiv \int_{-x/(2k|c_s|)}^{\eta_1} d\eta_2. \quad (2.50)$$

In the first case among these two the associated momentum integral is $(\int dp_1 dp_2)_1$, while it is $(\int dp_1 dp_2)_2$ in the latter. All in all, the complete loop integral may be decomposed in terms of these definitions as

$$\mathcal{I} = \left(\int d\eta_1 \right)_1 \left(\int d\eta_2 \right)_1 \left(\int dp_1 dp_2 \right)_1 + \left(\int d\eta_1 \right)_2 \left[\left(\int d\eta_2 \right)_2 \left(\int dp_1 \int dp_2 \right)_1 + \left(\int d\eta_2 \right)_3 \left(\int dp_1 dp_2 \right)_2 \right]. \quad (2.51)$$

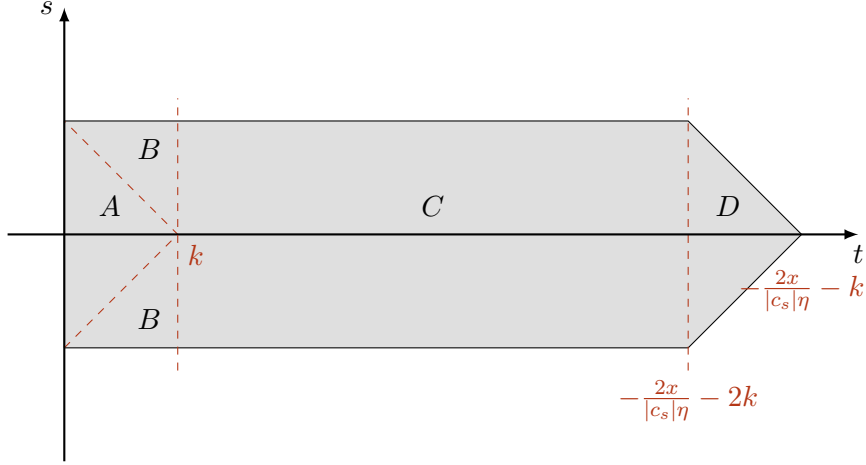


Figure 3. The integration domain for the momentum integrals in the loop diagram with two cubic vertices, in the (t, s) plane (cf. (2.53)). The gray region corresponds to the domain after introducing the EFT cutoff, which may be divided into four parts (A, B, C and D) for the purpose of calculating the integrals (see the main text for the rationale behind this division).

This result gives a correct definition of the loop integral in accordance with the cutoff prescription we have assumed. However, as we already mentioned, for practical purposes it is useful to exchange the order of integration. Performing the time integrals first, we have the limits of integration as given by

$$\eta_0 \equiv \max \left\{ -\frac{x}{k|c_s|}, -\frac{x}{p_1|c_s|}, -\frac{x}{p_2|c_s|} \right\} < \eta_2 < \eta_1 < \eta, \quad (2.52)$$

and the upper bound on each momentum integral is $-x/(|c_s|\eta)$.

Both for practical convenience and to better understand the structure of the momentum integrals, we introduce the variables

$$t \equiv p_1 + p_2 - k, \quad s \equiv p_1 - p_2, \quad (2.53)$$

and note that the Jacobian of the transformation is $1/2$, i.e. $\int dp_1 dp_2 = \frac{1}{2} \int dt ds$. Notice that $-k < s < k$ and $0 < t < -2x/(|c_s|\eta) - k$, however the integration domain is not rectangular, because $t + s < -2x/(|c_s|\eta) - k$ and $t - s < -2x/(|c_s|\eta) - k$; see Fig. 3.

The domain may be divided into three main parts depending on η_0 (cf. (2.52)).

- Region A is defined by the case $\eta_0 = -x/(k|c_s|)$, equivalently $p_1, p_2 < k$, i.e. $t + s < k$ and $t - s < k$. The loop integral in this region is given by

$$\mathcal{I}_A = \frac{1}{2} \int_0^k dt \int_{t-k}^{k-t} ds \int_{-x/(k|c_s|)}^{\eta} d\eta_1 \int_{-x/(k|c_s|)}^{\eta_1} d\eta_2. \quad (2.54)$$

- Region B has $p_1 + p_2 < 2k$, with either $p_1 > k$ or $p_2 > k$. Equivalently, $t < k$, and $t + s > k$ or $t - s > k$. The resulting loop integral is given by

$$\begin{aligned} \mathcal{I}_B = \frac{1}{2} \int_0^k dt \left[\int_{-k}^{t-k} ds \int_{-x/(p_2|c_s|)}^{\eta} d\eta_1 \int_{-x/(p_2|c_s|)}^{\eta_1} d\eta_2 \right. \\ \left. + \int_{k-t}^k ds \int_{-x/(p_1|c_s|)}^{\eta} d\eta_1 \int_{-x/(p_1|c_s|)}^{\eta_1} d\eta_2 \right]. \end{aligned} \quad (2.55)$$

- Region C has $2k < p_1 + p_2 < -2x/(|c_s|\eta) - k$, with either $p_1 > k$ or $p_2 > k$, or both $p_1, p_2 > k$. Equivalently, $k < t < -2x/(|c_s|\eta) - 2k$, and η_0 is determined by the sign of s . The corresponding loop integral is given by

$$\mathcal{I}_C = \frac{1}{2} \int_k^{-2x/(|c_s|\eta) - 2k} dt \left[\int_0^k ds \int_{-x/(p_1|c_s|)}^\eta d\eta_1 \int_{-x/(p_1|c_s|)}^{\eta_1} d\eta_2 \right. \\ \left. + \int_{-k}^0 ds \int_{-x/(p_2|c_s|)}^\eta d\eta_1 \int_{-x/(p_2|c_s|)}^{\eta_1} d\eta_2 \right]. \quad (2.56)$$

- Region D has $p_1 + p_2 > -2x/(|c_s|\eta) - k$, with $p_1, p_2 < -x/(|c_s|\eta)$ as per the EFT bound, and again η_0 is determined by the sign of s . The loop integral in this domain reads

$$\mathcal{I}_D = \frac{1}{2} \int_{-2x/(|c_s|\eta) - 2k}^{-2x/(|c_s|\eta) - k} dt \left[\int_0^{-2x/(|c_s|\eta) - k - t} ds \int_{-x/(p_1|c_s|)}^\eta d\eta_1 \int_{-x/(p_1|c_s|)}^{\eta_1} d\eta_2 \right. \\ \left. + \int_{2x/(|c_s|\eta) + k + t}^0 ds \int_{-x/(p_2|c_s|)}^\eta d\eta_1 \int_{-x/(p_2|c_s|)}^{\eta_1} d\eta_2 \right]. \quad (2.57)$$

3 One-loop scalar power spectrum

3.1 Loops with two cubic vertices

Having discussed the necessary calculational machinery, we are now ready to compute scalar one-loop diagrams in the in-in formalism. In this subsection we consider diagrams with two insertions of the cubic Hamiltonians $H_{\zeta\zeta\zeta}^{(1)}$ and $H_{\zeta\zeta\zeta}^{(2)}$ displayed in (2.27) and (2.28).

Two $H_{\zeta\zeta\zeta}^{(1)}$ -vertices.

We substitute $H_{\zeta\zeta\zeta}^{(1)}$ into the in-in formula (2.35) and carry out the Wick contractions (36 in total, all equivalent) to eventually obtain⁶

$$\langle \zeta_{\mathbf{k}}(\eta) \zeta_{\mathbf{p}}(\eta) \rangle = -\frac{144\mathcal{C}^2}{H^2} \delta^3(\mathbf{k} + \mathbf{p}) \int_{\eta_0}^\eta d\eta_1 \eta_1^{-1} \int_{\eta_0}^{\eta_1} d\eta_2 \eta_2^{-1} \int d^3\mathbf{p}_1 d^3\mathbf{p}_2 \delta^3(\mathbf{p}_1 + \mathbf{p}_2 - \mathbf{k}) \\ \times \text{Im} [\zeta'_k(\eta_1) \zeta_k^*(\eta)] \text{Im} [\zeta_k(\eta) \zeta_k^{*'}(\eta_2) \zeta'_{p_1}(\eta_1) \zeta_{p_1}^{*'}(\eta_2) \zeta'_{p_2}(\eta_1) \zeta_{p_2}^{*'}(\eta_2)]. \quad (3.1)$$

So far no approximation has been made. Next we consider the dominant contribution in the large- x expansion, which we find to correspond to the case when the two *internal* modes carrying the external momentum \mathbf{k} are decaying, i.e. $\zeta_k(\eta_1) = \zeta_{k,-}(\eta_1)$ and $\zeta_k(\eta_2) = \zeta_{k,-}(\eta_2)$, with all other fluctuations being growing modes; see Fig. 4 for an illustration. Notice that indeed at least two modes must be decaying, for otherwise the imaginary parts in the previous equation would evaluate to zero. Certainly, there are several other choices for the decaying modes, but we have found through an explicit calculation⁷ that the aforementioned choice

⁶Notice that we do not include contractions corresponding to tadpole diagrams (cf. Fig. 4). Indeed, contributions from tadpole diagrams vanish identically for purely derivative interactions [100], as considered in this paper. The simple reason is that a tadpole diagram includes a propagator with zero momentum, while time and spatial derivatives of the mode function vanish at zero momentum.

⁷Although our analytical results are restricted to the leading order contributions for each type of loop diagram, in every case we have checked through numerical computations that the neglected terms are indeed subleading.

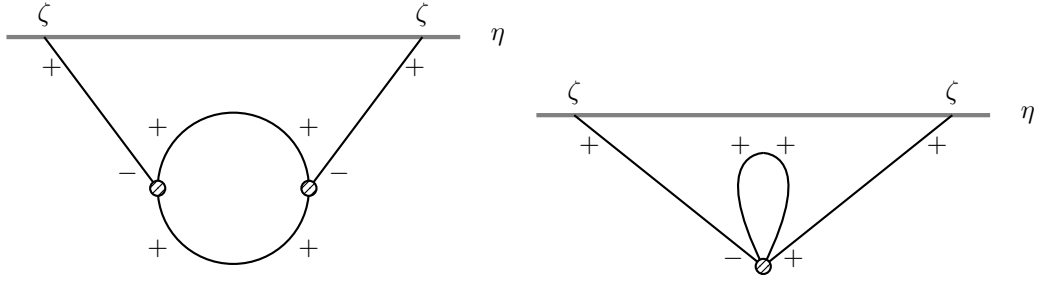


Figure 4. Leading scalar one-loop diagrams in the large- x approximation. The sign \pm associated with each mode indicates if it is growing or decaying, see Eq. (2.7).

gives the leading terms, namely ones proportional to x^5 , x^4 and x^3 in the final normalized result (see below), while other choices contribute at most at order x^2 .

Focusing on this choice, we then arrive at the following expression for the one-loop dimensionless power spectrum:

$$\frac{k^3}{2\pi^2} \langle \zeta^2 \rangle' = \frac{144 |c_s|^{12} \mathcal{C}^2}{\pi H^2} A^6 \text{Im}[B]^2 e^{2k|c_s|\eta} (k|c_s|\eta - 1)^2 \mathcal{I}_{\zeta\zeta\zeta}^{(1)}, \quad (3.2)$$

in terms of the integral

$$\begin{aligned} \mathcal{I}_{\zeta\zeta\zeta}^{(1)} &= \int_{\eta_0}^{\eta} d\eta_1 \int_{\eta_0}^{\eta_1} d\eta_2 \int_0^{\infty} dp_1 \int_{|p_1-k|}^{p_1+k} dp_2 \eta_1^2 \eta_2^2 p_1^2 p_2^2 e^{(p_1+p_2-k)|c_s|(\eta_1+\eta_2)} \\ &= \frac{1}{32} \int_{\eta_0}^{\eta} d\eta_1 \int_{\eta_0}^{\eta_1} d\eta_2 \int_0^{\infty} dt \int_{-k}^k ds \eta_1^2 \eta_2^2 \left((t+k)^2 - s^2 \right)^2 e^{t|c_s|(\eta_1+\eta_2)}. \end{aligned} \quad (3.3)$$

Next we regularize and manipulate this integral following the steps explained in the previous section. Before quoting the exact, analytical result, let us note that the dominant scaling with x may be inferred without carrying out the computation explicitly. First of all, the exponent of $e^{t|c_s|(\eta_1+\eta_2)}$ sets the dominant scale $-t|c_s|(\eta_1+\eta_2) \sim 1 \Rightarrow t \sim \frac{-1}{|c_s|(\eta_1+\eta_2)} \lesssim -2x/(|c_s|\eta_{1,2})$, where $-2x/(|c_s|\eta_{1,2})$ is roughly the upper bound on t . Then x enters in the result only through the lower limit η_0 of the time integrals. Consider first the contribution from region A (cf. Fig. 3), where the integrals are dominated by $\eta_1 \sim \eta_2 \sim -x/(k|c_s|)$. This leads to $t \sim k/x \ll k$, that is, the dominant contribution happens at the limit $p_1+p_2-k \sim k/x \ll k$. Setting $t \sim k/x$ and $\eta_1 \sim \eta_2 \sim -x/(k|c_s|)$, one immediately sees that the integral scales as $\mathcal{I}_{\zeta\zeta\zeta,A}^{(1)} \propto x^5$ (noting that the integration measures $\int dt$ and $\int d\eta_{1,2}$ contribute factors of order k/x and $-x/k|c_s|$, respectively). On the other hand, in regions B , C and D , we would have different dominant scales, namely $\eta_1, \eta_2 \sim -x/(p_{1,2}|c_s|)$, i.e. $t \sim p_{1,2}/x \ll k$ and $s \sim k$. These parts of the integral thus scale as x^2 and are therefore subdominant. We conclude then that the leading contribution to the integral comes from the domain A : $\mathcal{I}_{\zeta\zeta\zeta}^{(1)} = \mathcal{I}_{\zeta\zeta\zeta,A}^{(1)} + \mathcal{O}(x^2)$.

An explicit calculation confirms this quick estimate. Recalling the expressions for the parameters A , B and \mathcal{C} , as well as the dimensionless tree-level power spectrum \mathcal{P}_{ζ} , we eventually get

$$\boxed{\frac{k^3}{2\pi^2} \langle \zeta^2 \rangle' = \mathcal{P}_{\zeta}^2 \mathcal{A}^2 \left(\frac{1}{|c_s|^2} + 1 \right)^2 e^{2k|c_s|\eta} (k|c_s|\eta - 1)^2 \times \left[\frac{3(2 \log 2 - 1)}{800} x^5 + \frac{3(3 - 4 \log 2)}{128} x^4 + \frac{8 \log 2 - 5}{96} x^3 + \mathcal{O}(x^2) \right]}. \quad (3.4)}$$

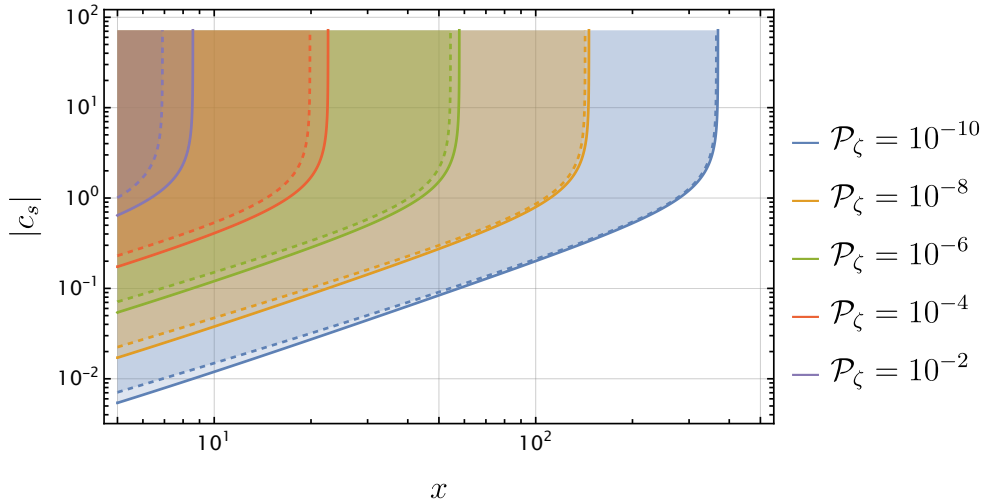


Figure 5. Consistency with perturbativity as dictated by the criterion $\mathcal{P}_\zeta^{(1\text{-loop})}/\mathcal{P}_\zeta^{(\text{tree})} < 1$ (colored regions) as function of x and $|c_s|$, for several values of \mathcal{P}_ζ (the tree-level dimensionless power spectrum). *Solid lines:* $\mathcal{P}_\zeta^{(1\text{-loop})}$ as given by Eq. (3.4) with $\mathcal{A} = 1$, i.e. the case of the diagram with two insertions of $H_{\zeta\zeta\zeta}^{(1)}$. *Dashed lines:* The same in the case of the loop diagram with two insertions of $H_{\zeta\zeta\zeta}^{(2)}$, cf. Eq. (3.6). Note that in both cases the late-time limit $\eta \rightarrow 0^-$ has been taken.

Remarkably, the integral $\mathcal{I}_{\zeta\zeta\zeta}^{(1)}$ is time-independent at the orders shown in the large- x expansion, although we emphasize that subdominant terms, starting at $\mathcal{O}(x^2)$, do depend on the external time η .

Defining $\mathcal{P}_\zeta^{(1\text{-loop})} \equiv \lim_{\eta \rightarrow 0^-} \frac{k^3}{2\pi^2} \langle \zeta^2 \rangle'$, one finds a simple expression for the ratio $\mathcal{P}_\zeta^{(1\text{-loop})}/\mathcal{P}_\zeta^{(\text{tree})}$ that we use to diagnose the breakdown of perturbativity. Taking $\mathcal{A} \sim 1$ one has

$$\frac{\mathcal{P}_\zeta^{(1\text{-loop})}}{\mathcal{P}_\zeta^{(\text{tree})}} \sim \mathcal{P}_\zeta \left(\frac{1}{|c_s|^2} + 1 \right)^2 x^5. \quad (3.5)$$

We see that this can be dangerously large already for moderate values of x . For example, using the CMB value $\mathcal{P}_\zeta \sim 10^{-9}$ and $|c_s| \sim 10^{-1}$, one has $\mathcal{P}_\zeta^{(1\text{-loop})}/\mathcal{P}_\zeta^{(\text{tree})} \sim 1$ for $x \sim 10$. On the positive side, models that predict $|c_s| = \mathcal{O}(1)$, such as hyper-inflation [52, 64], appear to be consistent even for values of \mathcal{P}_ζ that are strongly enhanced relative to CMB scales. A more precise illustration is provided in Fig. 5, where we show the “exclusion” region $\mathcal{P}_\zeta^{(1\text{-loop})}/\mathcal{P}_\zeta^{(\text{tree})} > 1$ as function of x and $|c_s|$ for several values of \mathcal{P}_ζ .⁸

Two $H_{\zeta\zeta\zeta}^{(2)}$ -vertices.

The second contribution we consider is the loop diagram with two insertions of the $H_{\zeta\zeta\zeta}^{(2)}$ Hamiltonian in Eq. (2.28). The calculation follows precisely the same steps as in the previous paragraph, the only additional complication being that there are now several inequivalent permutations. We provide details of the computation in Appendix B, while here we only

⁸Unlike in the standard situation with real c_s , here we have no fundamental obstruction for allowing $|c_s| > 1$. Note that this helps too much with the issue of perturbativity, since for large $|c_s|$ the bound then becomes degenerate in $|c_s|$.

quote the final result:

$$\frac{k^3}{2\pi^2} \langle \zeta^2 \rangle' = \mathcal{P}_\zeta^2 \left(\frac{1}{|c_s|^2} + 1 \right)^2 e^{2k|c_s|\eta} (k|c_s|\eta - 1)^2 \times \left[\frac{3(2 \log 2 - 1)}{800} x^5 + \frac{4 \log 2 + 5}{640} x^4 + \frac{16 \log 2 - 19}{480} x^3 + \mathcal{O}(x^2) \right]. \quad (3.6)$$

We remark on the close similarity of this result with the case of two $H_{\zeta\zeta\zeta}^{(1)}$ -vertices, Eq. (3.4). In particular, both feature the same x^5 dominance in the large- x approximation, which indeed can be explained through a simple scaling argument; see the next paragraph. We also observe the same $1/|c_s|^4$ enhancement in the limit of small $|c_s|$, consistent with our claim that the perturbativity bound is not qualitatively affected by considering all types of vertices. This is further illustrated in Fig. 5 displaying the exclusion regions as functions of x , $|c_s|$ and \mathcal{P}_ζ .

Two mixed vertices.

We have not carried out the calculation of the loop diagram with one insertion of $H_{\zeta\zeta\zeta}^{(1)}$ and one insertion of $H_{\zeta\zeta\zeta}^{(2)}$, a cumbersome task due to the large number of inequivalent permutations. Nevertheless, from the previous results one can clearly anticipate a qualitatively identical outcome, so that the full result will not be affected, in order of magnitude, from our neglecting this contribution.

Indeed, the scaling argument discussed previously applies generally to all the cubic vertices in the EFT of inflation in the regime we are considering. The only novelty here, compared to the easiest case with two insertions of $H_{\zeta\zeta\zeta}^{(1)}$, is that the $H_{\zeta\zeta\zeta}^{(2)}$ vertex carries both time and space derivatives of the mode function. Notice however that, as far as the exponential term in the integral is concerned (cf. (3.3)), time and space derivatives contribute equally, so the dominant scale is still set by $t \sim \frac{-1}{|c_s|(\eta_1 + \eta_2)}$. Powers of internal momenta therefore do not yield additional powers of x in this subdomain of integration. This explains why both of our explicit results, Eqs. (3.4) and (3.6), feature the same large- x scaling, and we similarly conclude that the terms we have neglected must also enjoy the same x^5 enhancement.

3.2 Loops with one quartic vertex

We move on to study one-loop diagrams with a single quartic vertex. Recall from Sec. 2 that we will consider for simplicity only the contribution from the ζ'^4 vertex given in (2.30), since neglecting other terms will not affect the result qualitatively, in particular concerning the large- x behavior; see Appendix C for further explanations as well as the explicit result for the $(\partial\zeta)^4$ vertex.

The relevant in-in integral is given in (2.36), into which we substitute $H_{\zeta\zeta\zeta\zeta}^{(1)}$ to produce

$$\langle \zeta_{\mathbf{k}}(\eta) \zeta_{\mathbf{p}}(\eta) \rangle = -24 \mathcal{D} \delta^3(\mathbf{k} + \mathbf{p}) \int_{\eta_0}^{\eta} d\eta_1 \int d^3 \mathbf{p}_1 \text{Im} \left[\zeta'_k(\eta_1) \zeta_k^*(\eta) \zeta'_k(\eta_1) \zeta_k^*(\eta) \zeta'_{p_1}(\eta_1) \zeta_{p_1}^*(\eta) \right], \quad (3.7)$$

after performing the Wick contractions and taking into account the 12 equivalent permutations. In order to isolate the leading behavior in the large- x approximation, it is clear that now it suffices to take only one of the modes to be decaying. We find that choosing either of the internal modes carrying the external momentum \mathbf{k} yields the dominant contribution,

i.e. $\zeta_k(\eta_1) = \zeta_{k,-}(\eta_1)$, just like in the case of the loop diagrams with two cubic vertices; this is also illustrated in Fig. 4. Eventually we obtain the following result for the contribution of this loop diagram to the dimensionless power spectrum:

$$\frac{k^3}{2\pi^2} \langle \zeta^2 \rangle' = -\frac{96|c_s|^8 \mathcal{D}}{\pi} A^5 \text{Im}[B] k e^{2k|c_s|\eta} (k|c_s|\eta - 1)^2 \mathcal{I}_{\zeta\zeta\zeta\zeta}, \quad (3.8)$$

where

$$\mathcal{I}_{\zeta\zeta\zeta\zeta} = \int_{\eta_0}^{\eta} d\eta_1 \int_0^{\infty} dp_1 \eta_1^4 p_1^3 e^{2p_1|c_s|\eta_1}. \quad (3.9)$$

This integral must be regularized following the prescription described in Sec. 2. As we have seen, this procedure introduces an explicit dependence on the cutoff parameter x , which is easy to estimate by means of the scaling argument we have already used. The exponential term $e^{2p_1|c_s|\eta_1}$ suppresses the integral except in the subdomain $-p_1|c_s|\eta_1 = \mathcal{O}(1)$; in this region, then, the integrand is independent of x , so the time integral yields $\int_{-x/(k|c_s|)}^{\eta} d\eta_1 \mathcal{O}(x^0) \propto x$, i.e. a linear scaling with x at leading order.

This quick estimate is borne out by an explicit computation of the integral:

$$\boxed{\frac{k^3}{2\pi^2} \langle \zeta^2 \rangle' = -\mathcal{P}_{\zeta}^2 \mathcal{D} e^{2k|c_s|\eta} (k|c_s|\eta - 1)^2 \left[\frac{9x}{4|c_s|^4} + \mathcal{O}(x^0) \right]}. \quad (3.10)$$

We have only quoted the $\propto x$ term since at $\mathcal{O}(x^0)$ we also have contributions from other combinations of growing versus decaying modes that we neglected. We remark that (3.10) features the same time dependence of the diagrams we computed previously, Eqs. (3.4) and (3.6). We emphasize however that this only holds at leading order in x , i.e. the $\mathcal{O}(x^0)$ terms that we omitted in (3.10) do depend on time and we do not expect this agreement to uphold at subleading orders.

In the late-time limit, and assuming $\mathcal{D} \sim 1$, we have the estimate

$$\frac{\mathcal{P}_{\zeta}^{(1\text{-loop})}}{\mathcal{P}_{\zeta}^{(\text{tree})}} \sim \mathcal{P}_{\zeta} \frac{x}{|c_s|^4}, \quad (3.11)$$

for the effect of the one-loop power spectrum, for this particular vertex, relative to the tree-level result. We observe that this is subleading in comparison with the contributions from diagrams with two cubic vertices in the large- x expansion, at least assuming $|c_s|$ is not too small. We show in Appendix C that other quartic vertices should have the same large- x behavior and are therefore also negligible in this approximation.

3.3 Counterterms and higher derivative corrections

We make an aside here to comment on the question of whether the one-loop results we have computed are actually physical. In standard QFT one knows that, in cutoff regularization, powers of the cutoff are unphysical since they are absorbed by counterterms upon renormalization. It is then natural to ask if the same might happen in the EFT of inflation with imaginary speed of sound.

As a first approach to this question, we can compute the effect of higher-derivative corrections that could a priori serve as counterterms in the renormalization procedure. This

has been done explicitly in Ref. [100] in the context of the standard EFT of inflation. Here we focus for simplicity on a single higher-derivative operator:

$$S_{\text{ct}} = \mathcal{K} \int d\eta d^3\mathbf{x} a^{-2} (\zeta''')^2, \quad (3.12)$$

where \mathcal{K} is a constant. There are actually two other terms at this order in the derivative expansion [100], however we have checked that they yield similar results and hence do not affect the reasoning that follows.

Treating (3.12) as an interaction in the in-in formalism, we find its contribution to the scalar power spectrum to be

$$\langle \zeta_{\mathbf{k}}(\eta) \zeta_{\mathbf{p}}(\eta) \rangle_{\text{ct}} = 4\mathcal{K}(2\pi)^3 \delta^3(\mathbf{k} + \mathbf{p}) \int_{\eta_0}^{\eta} d\eta_1 a^{-2}(\eta_1) \text{Im} [\zeta_k'''(\eta_1)^2 \zeta_k^*(\eta)^2]. \quad (3.13)$$

Regularizing the integral and isolating the leading terms in the large- x approximation, we eventually obtain

$$\begin{aligned} \frac{k^3}{2\pi^2} \langle \zeta^2 \rangle'_{\text{ct}} &= 16\pi^2 \mathcal{K} H^2 \mathcal{P}_{\zeta}^2 e^{-2x} |c_s|^3 (\rho \sin \psi) e^{2k|c_s|\eta} (k|c_s|\eta - 1)^2 \\ &\times \left[\frac{x^5}{5} - \frac{4x^3}{3} + \rho \cos \psi \left(\frac{x^4}{2} + x^3 \right) + \mathcal{O}(x^2) \right]. \end{aligned} \quad (3.14)$$

To get this result we have again considered the case when the two external modes are growing, which one can easily verify to produce the greatest enhancement in powers of x .⁹

A few remarks are in order. First, (3.14) features the same dependence on the external time η as the one-loop results, cf. (3.4), (3.6) and (3.10). However, as already explained, this is simply a consequence of our focusing on the contributions where the two external modes are growing. Since by assumption the external time is taken to be late enough, the dependence on η brought in by the time integral is necessarily subleading. So the agreement of (3.14) and the one-loop effects with regards to the time dependence should not be taken as a sign that the latter are unphysical. One could, of course, attempt to cancel these one-loop corrections by appropriately choosing the constant \mathcal{K} , however this can never be done for all times η and for all powers of x , so there is no reason why precisely the highest powers must be canceled via this procedure. In standard renormalization, *all* power-law divergences must be canceled, precisely because they are unphysical. We thus conclude that powers of x in our set-up are perfectly physical; in fact, they already appear at tree level [59, 64]. A second observation is that (3.14) is actually exponentially suppressed in the large- x approximation. This is both satisfactory, as it means that higher-derivative corrections do not contaminate our one-loop estimates, and also consistent with our claim that the latter effects are physical: in order for (3.14) to cancel the one-loop results, the constant \mathcal{K} must scale as e^{2x} . While formally nothing prevents one from making this choice, it would be again at odds with the standard logic of renormalization, where counterterms precisely absorb power-law divergences, but one does not encounter for instance exponentials of the cutoff.

⁹Unlike in the loop computations, we have considered here also the next-to-leading order combination of growing versus decaying modes, namely the case where two internal modes are decaying, which notably enter here at $\mathcal{O}(x^4)$.

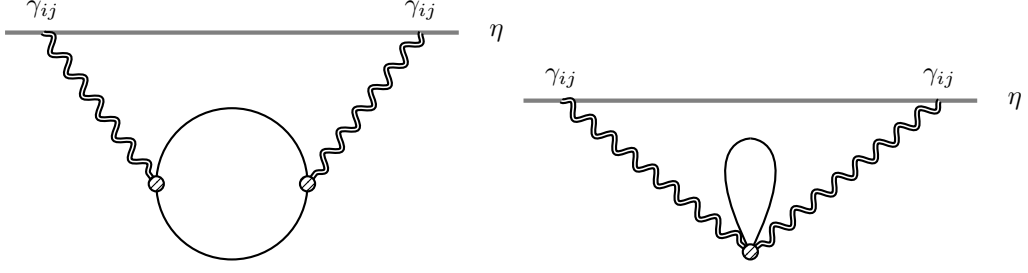


Figure 6. One-loop diagrams that contribute to the tensor power spectrum. Tensor modes are denoted by double-wiggly lines.

4 One-loop tensor power spectrum

In this Section we study the scalar one-loop corrections to the tensor power spectrum, focusing on the vertices listed in (2.29), (2.31) and (2.32). The two types of loop diagrams are shown in Fig. 4. A key difference relative to the scalar spectrum case of the previous Section is that here we may take all ζ modes as growing, with a correspondingly dangerous enhancement in the large- x regime.

4.1 Loops with two cubic vertices

As explained, at the order we are working in the slow-roll and derivative expansions, there is a single mixed scalar-tensor cubic vertex, Eq. (2.29). The relevant in-in integral is given in (2.35), of course replacing $\hat{\zeta}$ with $\hat{\gamma}$ in the external modes. Performing the Wick contractions we get

$$\begin{aligned}
\langle \gamma_{ij,\mathbf{k}}(\eta) \gamma_{ij,\mathbf{p}}(\eta) \rangle &= -16\mathcal{E}^2 P_{kl,mn}(\hat{\mathbf{k}}) \delta^3(\mathbf{k} + \mathbf{p}) \\
&\times \int_{-\infty}^{\eta} d\eta_1 a^2(\eta_1) \int_{-\infty}^{\eta_1} d\eta_2 a^2(\eta_2) \int d^3\mathbf{p}_1 \int d^3\mathbf{p}_2 \delta^3(\mathbf{p}_1 + \mathbf{p}_2 - \mathbf{k}) \\
&\times \mathbf{p}_1^k \mathbf{p}_2^l \mathbf{p}_1^m \mathbf{p}_2^n \text{Im} [\gamma_k(\eta_1) \gamma_k^*(\eta)] \text{Im} [\zeta_{p_1}(\eta_1) \zeta_{p_1}^*(\eta_2) \zeta_{p_2}(\eta_1) \zeta_{p_2}^*(\eta_2) \gamma_k(\eta) \gamma_k^*(\eta_2)] .
\end{aligned} \tag{4.1}$$

Recall that the tensor mode functions are given by the Bunch-Davies state, while for the scalar fluctuations we isolate the leading behavior in x by considering only growing modes. Thus we arrive at¹⁰

$$\begin{aligned}
\frac{k^3}{2\pi^2} \langle \gamma^2 \rangle' &= -\frac{4\epsilon^2 \mathcal{P}_{\zeta}^2}{k^2} \int_{-\infty}^{\eta} \frac{d\eta_1}{\eta_1^2} \int_{-\infty}^{\eta_1} \frac{d\eta_2}{\eta_2^2} e^{-ik(2\eta - \eta_1 - \eta_2)} \\
&\times \left(e^{2ik(\eta - \eta_1)} (i + k\eta)(-i + k\eta_1) - (-i + k\eta)(i + k\eta_1) \right) \\
&\times \left(e^{2ik(\eta - \eta_2)} (i + k\eta)(-i + k\eta_2) - (-i + k\eta)(i + k\eta_2) \right) \\
&\times \int_0^{\infty} du \int_{|1-u|}^{1+u} dv \left[\frac{4v^2 - (1 + v^2 - u^2)^2}{4uv} \right]^2 e^{(u+v)k|c_s|(\eta_1 + \eta_2)} \\
&\times (uk|c_s|\eta_1 - 1)(uk|c_s|\eta_2 - 1)(vk|c_s|\eta_1 - 1)(vk|c_s|\eta_2 - 1) ,
\end{aligned} \tag{4.3}$$

¹⁰Here we made use of the identity

$$P_{ij,kl}(\hat{\mathbf{k}}) \mathbf{p}_1^i \mathbf{p}_2^j \mathbf{p}_1^k \mathbf{p}_2^l = \frac{1}{2} [p_1^2 - (\mathbf{p}_1 \cdot \hat{\mathbf{k}})^2] [p_2^2 - (\mathbf{p}_2 \cdot \hat{\mathbf{k}})^2] . \tag{4.2}$$

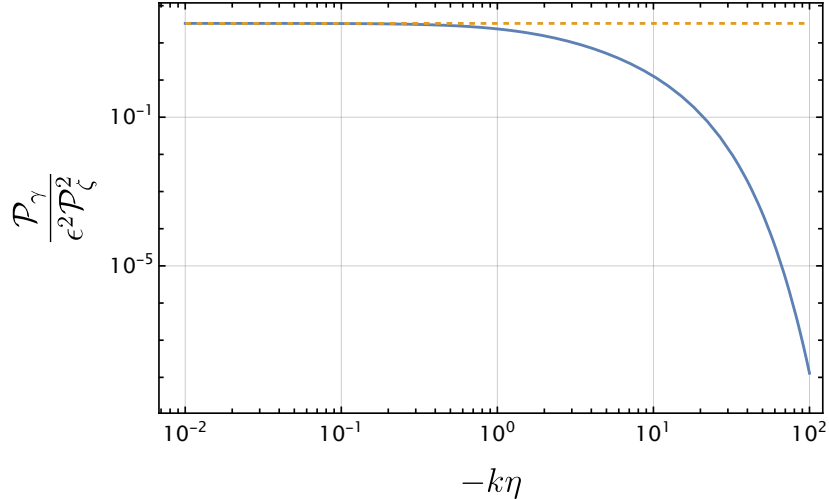


Figure 7. Time evolution of the one-loop correction $\mathcal{P}_\gamma^{(1\text{-loop})}$ from the cubic vertex $H_{\gamma\zeta\zeta}$, at leading order in the large- x approximation, i.e. Eq. (4.3), using $|c_s| = 10^{-1}$ and normalized by $\epsilon^2 \mathcal{P}_\zeta^2$. The horizontal dashed line is the late-time limit given by Eq. (4.4).

where we introduced the variables $u \equiv p_1/k$ and $v \equiv p_2/k$. Observe that time integrals here are not cut off because the momentum of the tensor modes can be arbitrarily large. On the other hand, the momentum integrals relate to the momenta of the scalar modes running in the loop, and are therefore bounded by $-x/|c_s|\eta_2$. Remarkably, however, a quick inspection of the integral reveals that the result is actually independent of x at leading order in the large- x expansion. Equivalently, the limit $x \rightarrow \infty$ converges and captures this leading-order behavior. To see this, notice that the exponential term suppresses the integral except in the region around $u + v \sim -\frac{1}{k|c_s|(\eta_1 + \eta_2)}$, which is parametrically smaller than the upper bound on $u + v$, i.e. $-2x/(k|c_s|\eta_2)$. Put conversely, any x -dependence of the integral must arise from the upper limit of integration, near which the integrand is exponentially suppressed, $\exp[(u + v)k|c_s|(\eta_1 + \eta_2)] \lesssim e^{-x}$.

The integral in (4.3) can be performed analytically for any finite external time η , although the result is long and not particularly illuminating. We display the time evolution in Fig. 7, which shows that the loop correction grows monotonically with time and quickly approaches a constant value after horizon crossing. Evaluating at $\eta \rightarrow 0^-$ we obtain

$$\begin{aligned} \mathcal{P}_\gamma^{(1\text{-loop})} = \frac{\epsilon^2 \mathcal{P}_\zeta^2}{45} & \left[-\frac{15|c_s|^4 + 364|c_s|^2 + 357}{1 + |c_s|^2} \right. \\ & \left. + \frac{3}{|c_s|} \left(\frac{\pi}{2} - \arctan |c_s| \right) (5|c_s|^4 + 118|c_s|^2 + 41) + \mathcal{O}(x^{-1}) \right]. \end{aligned} \quad (4.4)$$

The result in (4.4) looks very small, suppressed both by a power of the slow-roll parameter and by the scalar power spectrum. But this is deceiving, since what we are really interested in is the relative correction to the tree-level result,

$$\mathcal{P}_\gamma^{(\text{tree})} = \frac{2}{\pi^2} \left(\frac{H}{M_{\text{Pl}}} \right)^2 = 32\epsilon|c_s|(\rho \sin \psi) \mathcal{P}_\zeta e^{-2x}, \quad (4.5)$$

so that the ratio $\mathcal{P}_\gamma^{(1\text{-loop})}/\mathcal{P}_\gamma^{(\text{tree})}$ is exponentially enhanced when x is large. Fortunately, the ratio is still proportional to $\epsilon \mathcal{P}_\zeta$ and, at least on CMB scales, this can reasonably overcome

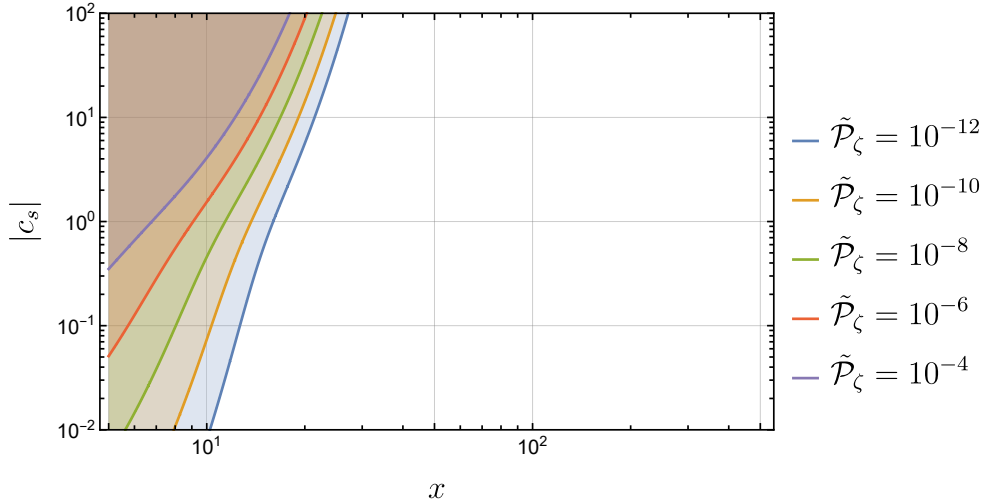


Figure 8. Consistency with perturbativity as dictated by the criterion $\mathcal{P}_\gamma^{(1\text{-loop})}/\mathcal{P}_\gamma^{(\text{tree})} < 1$ (colored regions) as function of x and $|c_s|$, for several values of $\tilde{\mathcal{P}}_\zeta \equiv \epsilon\mathcal{P}_\zeta/(\rho \sin \psi)$, with $\mathcal{P}_\gamma^{(1\text{-loop})}$ as given by Eq. (4.4), i.e. the case of the diagram with two insertions of $H_{\gamma\zeta\zeta}$.

the exponential term e^{2x} as long as $x \lesssim \mathcal{O}(10)$ (here we are assuming as usual that $\rho \sin \psi$ is of order unity). We display the perturbativity bound, as function of x , $|c_s|$ and \mathcal{P}_ζ , in Fig. 8.

Comment on higher loops.

Given the dangerously large result for $\mathcal{P}_\gamma^{(1\text{-loop})}$ that we have found, it is interesting to naively ask if this correction might actually dominate over the tree-level result while still being consistent with the loop expansion. That is, we ask if *higher* loop corrections could satisfy a consistent expansion even if $\mathcal{P}_\gamma^{(1\text{-loop})}/\mathcal{P}_\gamma^{(\text{tree})} > 1$. A quick back-of-the-envelope estimate shows however that this is not the case, i.e. a violation of our perturbativity bound derived at one-loop order really signals a breakdown of the full loop expansion.

Consider for concreteness a two-loop diagram with four insertions of the cubic Hamiltonian $H_{\gamma\zeta\zeta}$. The two-point correlator is given schematically by

$$\langle \gamma^2 \rangle^{(2\text{-loop})} \sim \mathcal{E}^4 \left\langle \left(a^2 \int \gamma\zeta\zeta \right)^2 \gamma^2 \left(a^2 \int \gamma\zeta\zeta \right)^2 \right\rangle \sim \epsilon^4 \left(\frac{M_{\text{Pl}}}{H} \right)^8 \mathcal{P}_\zeta^4 \mathcal{P}_\gamma^3. \quad (4.6)$$

Since $\langle \gamma^2 \rangle^{(1\text{-loop})} \sim \epsilon^2 \mathcal{P}_\zeta^2 \mathcal{P}_\gamma^2 (M_{\text{Pl}}/H)^4$, we have again that

$$\frac{\langle \gamma^2 \rangle^{(2\text{-loop})}}{\langle \gamma^2 \rangle^{(1\text{-loop})}} \sim \epsilon \mathcal{P}_\zeta e^{2x}. \quad (4.7)$$

Similarly, for all higher loops, we can estimate $\mathcal{P}_\gamma^{((n+1)\text{-loop})}/\mathcal{P}_\gamma^{(n\text{-loop})} \sim \mathcal{P}_\gamma^{(1\text{-loop})}/\mathcal{P}_\gamma^{(\text{tree})}$, consistent with expectations.

4.2 Loops with one quartic vertex

It remains to consider the one-loop corrections from diagrams with one quartic vertex, given by the interaction Hamiltonians $H_{\gamma\gamma\zeta\zeta}^{(1)}$ and $H_{\gamma\gamma\zeta\zeta}^{(2)}$, cf. Eqs. (2.31) and (2.32). It is easy to

convince oneself, before doing any calculation, that these contributions are actually totally safe with regards to the large- x expansion. Indeed, the in-in integral contains two fewer factors of ζ in comparison with the loop of the previous subsection, so we expect a suppression of e^{-2x} in $\mathcal{P}_\gamma^{(1\text{-loop})}$ in the present case. Nevertheless, it turns out that loops with quartic vertices introduce a new behavior, namely an infrared divergence associated to the late-time limit.

$H_{\gamma\zeta\zeta}^{(1)}$ -vertex.

Inserting (2.31) into the relevant in-in formula we obtain

$$\langle \gamma_{ij,\mathbf{k}}(\eta)\gamma_{ij,\mathbf{p}}(\eta) \rangle = -\frac{8\mathcal{F}}{H^2} \delta^3(\mathbf{k} + \mathbf{p}) \int_{-\infty}^{\eta} \frac{d\eta_1}{\eta_1^2} \int d^3\mathbf{p}_1 |\zeta'_{p_1}(\eta_1)|^2 \text{Im} [\gamma_k(\eta_1)\gamma_k^*(\eta)\gamma_k(\eta_1)\gamma_k^*(\eta)]. \quad (4.8)$$

Focusing as usual in the large- x approximation, we take the scalar modes as growing, resulting in the following expression for the dimensionless one-loop tensor spectrum:

$$\frac{k^3}{2\pi^2} \langle \gamma^2 \rangle' = -\frac{8\mathcal{F}\epsilon|c_s|^2}{k^3} \mathcal{P}_\zeta \mathcal{P}_\gamma \text{Im} \left[e^{2ik\eta} (i+k\eta)^2 \int_{-\infty}^{\eta} d\eta_1 \int_0^{\infty} dp_1 p_1^3 e^{2p_1|c_s|\eta_1 - 2ik\eta_1} (i-k\eta_1)^2 \right]. \quad (4.9)$$

The upper limit of the momentum integral should in principle be cutoff at $p_1 = -x/(|c_s|\eta_1)$. However, using a very similar argument as in the previous subsection, one can easily see that the integral in (4.9) is actually convergent at $p_1 \rightarrow \infty$. We conclude again that the leading-order result in the large- x expansion is independent of x and is precisely given by the above integral.

The integral (4.9) is on the other hand IR divergent, i.e. it diverges as $\log(-k\eta)$ as $\eta \rightarrow 0^-$,¹¹

$$\frac{k^3}{2\pi^2} \langle \gamma^2 \rangle' = \frac{2\epsilon\mathcal{F}\mathcal{P}_\zeta\mathcal{P}_\gamma}{|c_s|^2} [\log(-2k\eta) + \gamma_E - 2] + \mathcal{O}(\eta^2), \quad (4.10)$$

where γ_E is the Euler constant. Such secular divergences, arising from non-linear effects accumulating on super-Hubble scales, are commonplace in perturbative QFT in de Sitter space. However, there is never any infrared divergent correlator in actual inflationary models, simply because inflation had a finite duration; or equivalently, these divergences may be seen as artifacts of assuming perfect scale invariance. Hence it is sufficient for our purpose to simply regularize the result by introducing an IR cutoff $-k\eta_{\text{IR}} = \Lambda_{\text{IR}}/H$, corresponding to a time η_{IR} long after the mode k of interest exits the horizon, with the assumption $\Lambda_{\text{IR}} \ll H$. Evaluating the result one arrives at

$$\mathcal{P}_\gamma^{(1\text{-loop})} \simeq -\frac{2\epsilon\mathcal{F}\mathcal{P}_\zeta\mathcal{P}_\gamma}{|c_s|^2} \log \frac{H}{\Lambda_{\text{IR}}}, \quad (4.11)$$

where the approximate sign is because we are neglecting subleading terms in the large- x expansion, which are at least proportional to $1/x$, as well as IR-finite terms, i.e. terms which converge as $\Lambda_{\text{IR}} \rightarrow 0$.

As claimed, the ratio $\mathcal{P}_\gamma^{(1\text{-loop})}/\mathcal{P}_\gamma^{(\text{tree})}$ is independent of x at leading order, so this one-loop correction can be considered as safe from the point of view of perturbativity: even for reasonably large values of H/Λ_{IR} , the suppression by $\epsilon\mathcal{P}_\zeta \ll 1$ should ensure perturbative control.

¹¹We find it interesting that some non-trivial cancellations occur in order to produce this result. Indeed, the integral inside the imaginary part actually diverges as η^{-3} and η^{-1} as $\eta \rightarrow 0^-$. However, all such dangerous powers turn out to be purely real and hence do not contribute to the final result.

$H_{\gamma\gamma\zeta\zeta}^{(2)}$ -vertex.

The loop correction from the second interaction, Eq. (2.31), can be computed following the exact same procedure, with analogous results: finite in the large- x limit but logarithmically IR-divergent. We quote here only the final result:

$$\mathcal{P}_\gamma^{(1\text{-loop})} \simeq -\frac{6\epsilon\tilde{\mathcal{F}}\mathcal{P}_\zeta\mathcal{P}_\gamma}{|c_s|^2} \log \frac{H}{\Lambda_{\text{IR}}}. \quad (4.12)$$

5 Discussion

Our main aim in this paper was to address the question of whether the EFT of inflation with imaginary speed of sound admits a consistent loop expansion within the space of parameters of phenomenological interest, i.e. those found in concrete multi-field realizations such as strongly non-geodesic models of inflation characterized by a large and negative entropic mass m_s^2 .

At least generically, one expects the ratio of the one-loop correction of an observable to its tree-level value to give a good estimate of the parameter controlling the full loop expansion, cf. our discussion in Sec. 4.1. The simplest such observables in the present context are the scalar and tensor power spectra, which we treated in this paper, respectively in Sec. 3 and Sec. 4. Interestingly, we have found qualitatively distinct results depending on the type of one-loop diagram:

- Loop corrections to the scalar spectrum from diagrams with two cubic vertices provide the dominant contribution, of order $\mathcal{P}_\zeta^{(1\text{-loop})} \sim \mathcal{P}_\zeta^2 x^5$, ignoring numerical factors and $|c_s| \sim 1$. For small $|c_s|$, this is further enhanced by $|c_s|^{-4}$;
- Loop corrections to the scalar spectrum from diagrams with one quartic vertex give a subleading contribution, of order $\mathcal{P}_\zeta^{(1\text{-loop})} \sim \mathcal{P}_\zeta^2 x$ if $|c_s| \sim 1$, enhanced by $|c_s|^{-4}$ if $|c_s|$ is small;
- Loop corrections to the tensor spectrum from diagrams with two cubic vertices yield a dangerous, exponentially enhanced correction of order $\mathcal{P}_\gamma^{(1\text{-loop})}/\mathcal{P}_\gamma^{(\text{tree})} \sim \epsilon\mathcal{P}_\zeta e^{2x}$;
- Loop corrections to the tensor spectrum from diagrams with one quartic vertex are not at all enhanced by powers or exponentials of x . However, they exhibit a qualitative difference: they are logarithmically IR-divergent at late times.

As a technical aspect, our calculations required a careful manipulation of loop integrals, which in the EFT with imaginary sound speed must be regularized with a (time-dependent) cutoff on momenta. This procedure results in a non-trivial domain of integration for nested time and momentum integrals, implying in particular that care is needed when exchanging the order of integration. We have striven to describe this prescription in detail, as we expect that it may find application in other contexts involving loop calculations within the in-in formalism.

As mentioned repeatedly throughout the paper, our results and conclusions rely on the large- x approximation, which is a necessary condition for the EFT to capture the sub-sound horizon physics that produces the salient features of this class of models. In practice, it has been shown that $x = \mathcal{O}(10)$ is typically large enough for the EFT to correctly reproduce the predictions of the multi-field theory, at least in cases where the comparison can be investigated in detail [64]. Moreover, and importantly, x cannot be arbitrarily large, since in fact one has the bound $x \lesssim |m_s|/H$ as a requirement for the consistency of integrating out a heavy

tachyonic entropic field [59]. For instance, in the models of sidetracked inflation [58] with large entropic mass, one has $|c_s| \ll 1$ and $x \sim \eta_\perp \sim |m_s| |c_s| / H$ on dimensional grounds (see also [67]), consistent with the above bound.

It is worth commenting on the accuracy of our results. The first remark is that our regularization prescription, in which momentum integrals are bounded by a hard cutoff, is expected to provide a correct order of magnitude, although not necessarily an accurate result whenever there is a dependence on the cutoff. Remarkably, in this regard, our main result concerning the dominant contribution to the tensor spectrum is that this observable is actually independent of the cutoff, which we therefore expect to be more accurate than our corresponding results for the scalar power spectrum. The second comment concerns the possibility that some of our results may be potentially canceled by counterterms when the theory is renormalized. We have given several arguments in support of the tenet that our results do capture physical effects. Nevertheless, a more thorough answer to this question would require a rigorous understanding of how renormalization works in this theory, which we currently lack. Also interesting, although technically challenging, would be to compare our results with the calculation performed in a multi-field UV completion, following for instance the techniques developed in [21].

An important conclusion is that loop corrections can easily become dangerously large in the EFT with imaginary speed of sound. This is relevant both in the formal context of the EFT itself, but also in the context of strongly non-geodesic models of inflation, given that the question of perturbativity in the multi-field theory may be reliably diagnosed within the EFT, assuming of course one works within its regime of validity. The issue of large loops concerns particularly scenarios predicting a very large bending, say $x \gtrsim 100$, or ones that feature a strong enhancement of the scalar power spectrum on small scales. For instance, taking into consideration the perturbativity of the scalar power spectrum, cf. Fig. 5, we find that very large values of \mathcal{P}_ζ , e.g. $\mathcal{P}_\zeta \sim 10^{-2}$, appear to be inconsistent as soon as $x \gtrsim 10$, barring cancellations among different diagrams, a situation that is only worsened for small values of $|c_s|$.¹² On the other hand, it is an interesting result that this tension is mostly absent in models with $|c_s| = \mathcal{O}(1)$, at least provided x is not too large, which as we have remarked is a reasonable situation and is found in concrete multi-field realizations. It would be interesting to consider loop corrections to other observables to see whether our bounds can be tightened even further.

Acknowledgments

SGS acknowledges support from the NSFC (Grant No. 12250410250) and from a provincial grant (Grant No. 2023QN10X389). The work of YL was supported by the NSFC (Grant No. 12247161), by the China Postdoctoral Science Foundation (Grant No. 2022TQ0140) and by the SIMIS. During the course of this work, S.R.P. was supported by the European Research Council under the European Union’s Horizon 2020 research and innovation programme (grant agreement No. 758792, Starting Grant project GEODESI).

A Lowest-order EFT and k-inflation

We mentioned that our set-up is equivalent to the theory of fluctuations in the context of k-inflation [97, 98], i.e. the covariant scalar field model defined by a Lagrangian of the form

¹²This does not immediately rule out large values of \mathcal{P}_ζ if they were to also exhibit a strong scale dependence. It is worth recalling that all our results rest on the assumption of approximate scale-invariance.

$P(X, \phi)$, with $X \equiv -\frac{1}{2}(\nabla\phi)^2$, and P an arbitrary function. Although well known, this equivalence is not manifest due to the usual ambiguities related to boundary terms and field redefinitions, so we provide a brief review of this aspect here.

The cubic action for ζ in the EFT at lowest order in derivatives and in the slow-roll expansion is given by [85, 101]

$$S_{\zeta^3} = \int dt d^3\mathbf{x} a^3 \frac{\epsilon M_{\text{Pl}}^2}{H} \left(1 - \frac{1}{c_s^2}\right) \left[\frac{\mathcal{A}}{c_s^2} \dot{\zeta}^3 + \dot{\zeta} \frac{(\partial\zeta)^2}{a^2} \right]. \quad (\text{A.1})$$

We warn the reader that we use cosmic time t in this Appendix, unlike in the rest of the paper. Actually, we recall that the EFT of inflation starts life not with the curvature perturbation ζ , but with the Nambu-Goldstone boson of broken time translations, denoted by π . The two are related non-linearly as $\zeta = -H\pi + H\pi\dot{\pi} + \frac{1}{2}\dot{H}\pi^2 + \mathcal{O}(\pi^3)$ [102]. This point is immaterial as far as the cubic Lagrangian is concerned (substituting the non-linear terms in the quadratic action for ζ will generate cubic terms, but these are proportional to the linear equation of motion, which are irrelevant in a perturbative treatment), but it is important if one wishes to determine the precise coefficients of the quartic vertices. As explained in the main text, in this paper we were not concerned with calculating these coefficients (e.g. in terms of the defining coefficients of the EFT) but rather considered them as extra free parameters.

The standard form of the cubic action for ζ derived in k-inflation is given by [84]

$$S_{\zeta^3} = \int d\eta d^3\mathbf{x} a^3 \frac{\epsilon M_{\text{Pl}}^2}{c_s^2} \left\{ - \left[\left(1 - \frac{1}{c_s^2}\right) + \frac{2\lambda}{\Sigma} \right] \frac{\dot{\zeta}^3}{H} + 3 \left(1 - \frac{1}{c_s^2}\right) \zeta \dot{\zeta}^2 + (1 - c_s^2) \zeta \frac{(\partial\zeta)^2}{a^2} \right\}. \quad (\text{A.2})$$

remembering that we neglect subleading corrections in the slow-roll expansion. Here $\Sigma \equiv XP_X + 2X^2P_{XX} = \epsilon H^2/c_s^2$ and $\lambda \equiv X^2P_{XX} + \frac{2}{3}X^3P_{XXX}$ are defined in terms of X and partial derivatives of the function P (e.g. $P_X \equiv \frac{\partial P}{\partial X}$), all evaluated on the background. Although not obvious, (A.1) and (A.2) coincide up to boundary terms, with the identification $\mathcal{A}(1 - c_s^{-2}) = 2\lambda/\Sigma$ [63, 103].¹³

The difference between (A.1) and (A.2) is given explicitly by

$$- \int dt d^3\mathbf{x} \frac{d}{dt} \left[\frac{a\epsilon M_{\text{Pl}}^2}{Hc_s^2} (1 - c_s^2) \zeta (\partial\zeta)^2 + \frac{a^3\epsilon M_{\text{Pl}}^2}{Hc_s^4} (1 - c_s^2) \zeta \dot{\zeta}^2 \right] + \dots, \quad (\text{A.3})$$

where the ellipses stand for *spatial* boundary terms, which do not affect cosmological correlators. The first term inside the brackets does not contain $\dot{\zeta}$ and therefore does not contribute to correlation functions that include only fields (and not field momenta) [104, 105], while the second term does not contribute to these correlators because of the super-Hubble conservation of ζ .

B Scalar loop from $H_{\zeta\zeta\zeta}^{(2)}$

The calculation of the one-loop scalar spectrum with two insertions of the $H_{\zeta\zeta\zeta}^{(2)}$ vertex (cf. Eq. (2.28)) is made lengthy by the number of inequivalent permutations. In this Appendix we provide details of the computation which we preferred to avoid in the main text.

¹³Although here we are focusing only on the leading terms in the slow-roll expansion, we emphasize that the equivalence is valid at all orders in slow-roll. Incidentally, the relation $\mathcal{A}(1 - c_s^{-2}) = 2\lambda/\Sigma$ is exact and does not assume any slow-roll approximation.

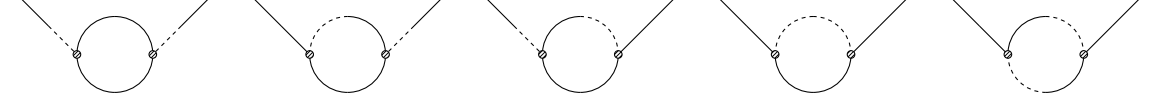


Figure 9. Five permutations for the one-loop diagram with two insertions of the cubic vertex $H_{\zeta\zeta\zeta}^{(2)}$. Dashed curves represent modes with time derivative.

There are five distinct permutations that contribute to the loop integral, as shown in Fig. 9; we label these, from left to right, as a, b, c, d, e . The individual contributions to the two-point correlator are given by

$$\begin{aligned}
\langle \zeta_{\mathbf{k}}(\eta)\zeta_{\mathbf{p}}(\eta) \rangle^{(a)} &= -\frac{16\tilde{\mathcal{C}}^2}{H^2}\delta^3(\mathbf{k}+\mathbf{p})\int d\eta_1\eta_1^{-1}\int d\eta_2\eta_2^{-1}\int d^3\mathbf{p}_1d^3\mathbf{p}_2\delta^3(\mathbf{p}_1+\mathbf{p}_2-\mathbf{k}) \\
&\quad \times (\mathbf{p}_1\cdot\mathbf{p}_2)^2\text{Im}[\zeta'_k(\eta_1)\zeta_k^*(\eta)]\text{Im}[\zeta_k(\eta)\zeta_k^{*\prime}(\eta_2)\zeta_{p_1}(\eta_1)\zeta_{p_1}^*(\eta_2)\zeta_{p_2}(\eta_1)\zeta_{p_2}^*(\eta_2)] \\
&= \frac{2\pi^2}{k^3}\delta^3(\mathbf{k}+\mathbf{p})\frac{8\tilde{\mathcal{C}}^2|c_s|^2}{\pi H^2}A^6\text{Im}[B]^2e^{2k|c_s|\eta}(k|c_s|\eta-1)^2 \\
&\quad \times \left[\frac{x^5}{150}(2\log 2-1) + \frac{x^4}{12}(2\log 2-1) + \frac{x^3}{12}(8\log 2-5) + \mathcal{O}(x^2) \right], \tag{B.1}
\end{aligned}$$

$$\begin{aligned}
\langle \zeta_{\mathbf{k}}(\eta)\zeta_{\mathbf{p}}(\eta) \rangle^{(b)} &= -\frac{32\tilde{\mathcal{C}}^2}{H^2}\delta^3(\mathbf{k}+\mathbf{p})\int d\eta_1\eta_1^{-1}\int d\eta_2\eta_2^{-1}\int d^3\mathbf{p}_1d^3\mathbf{p}_2\delta^3(\mathbf{p}_1+\mathbf{p}_2-\mathbf{k}) \\
&\quad \times (\mathbf{p}_1\cdot\mathbf{p}_2)(\mathbf{k}\cdot\mathbf{p}_2)\text{Im}[\zeta_k(\eta_1)\zeta_k^*(\eta)]\text{Im}[\zeta_k(\eta)\zeta_k^{*\prime}(\eta_2)\zeta'_{p_1}(\eta_1)\zeta_{p_1}^*(\eta_2)\zeta_{p_2}(\eta_1)\zeta_{p_2}^*(\eta_2)] \\
&= \frac{2\pi^2}{k^3}\delta^3(\mathbf{k}+\mathbf{p})\frac{16\tilde{\mathcal{C}}^2|c_s|^2}{\pi H^2}A^6\text{Im}[B]^2e^{2k|c_s|\eta}(k|c_s|\eta-1)^2 \\
&\quad \times \left[\frac{x^5}{150}(2\log 2-1) + \frac{13x^4}{240}(2\log 2-1) + \frac{x^3}{720}(224\log 2-197) + \mathcal{O}(x^2) \right], \tag{B.2}
\end{aligned}$$

$$\begin{aligned}
\langle \zeta_{\mathbf{k}}(\eta)\zeta_{\mathbf{p}}(\eta) \rangle^{(c)} &= -\frac{32\tilde{\mathcal{C}}^2}{H^2}\delta^3(\mathbf{k}+\mathbf{p})\int d\eta_1\eta_1^{-1}\int d\eta_2\eta_2^{-1}\int d^3\mathbf{p}_1d^3\mathbf{p}_2\delta^3(\mathbf{p}_1+\mathbf{p}_2-\mathbf{k}) \\
&\quad \times (\mathbf{p}_1\cdot\mathbf{p}_2)(\mathbf{k}\cdot\mathbf{p}_2)\text{Im}[\zeta'_k(\eta_1)\zeta_k^*(\eta)]\text{Im}[\zeta_k(\eta)\zeta_k^*(\eta_2)\zeta_{p_1}(\eta_1)\zeta_{p_1}^{*\prime}(\eta_2)\zeta_{p_2}(\eta_1)\zeta_{p_2}^*(\eta_2)] \\
&= \frac{2\pi^2}{k^3}\delta^3(\mathbf{k}+\mathbf{p})\frac{16\tilde{\mathcal{C}}^2|c_s|^2}{\pi H^2}A^6\text{Im}[B]^2e^{2k|c_s|\eta}(k|c_s|\eta-1)^2 \\
&\quad \times \left[\frac{x^5}{150}(2\log 2-1) - \frac{x^4}{120}(\log 2-4) + \frac{x^3}{720}(151-208\log 2) + \mathcal{O}(x^2) \right], \tag{B.3}
\end{aligned}$$

$$\begin{aligned}
\langle \zeta_{\mathbf{k}}(\eta)\zeta_{\mathbf{p}}(\eta) \rangle^{(d)} &= -\frac{32\tilde{\mathcal{C}}^2}{H^2}\delta^3(\mathbf{k}+\mathbf{p})\int d\eta_1\eta_1^{-1}\int d\eta_2\eta_2^{-1}\int d^3\mathbf{p}_1d^3\mathbf{p}_2\delta^3(\mathbf{p}_1+\mathbf{p}_2-\mathbf{k}) \\
&\quad \times (\mathbf{k}\cdot\mathbf{p}_2)^2\text{Im}[\zeta_k(\eta_1)\zeta_k^*(\eta)]\text{Im}[\zeta_k(\eta)\zeta_k^*(\eta_2)\zeta'_{p_1}(\eta_1)\zeta_{p_1}^{*\prime}(\eta_2)\zeta_{p_2}(\eta_1)\zeta_{p_2}^*(\eta_2)] \\
&= \frac{2\pi^2}{k^3}\delta^3(\mathbf{k}+\mathbf{p})\frac{16\tilde{\mathcal{C}}^2|c_s|^2}{\pi H^2}A^6\text{Im}[B]^2e^{2k|c_s|\eta}(k|c_s|\eta-1)^2 \\
&\quad \times \left[\frac{x^5}{150}(2\log 2-1) - \frac{x^4}{240}(16\log 2-15) + \frac{x^3}{120}(8\log 2-11) + \mathcal{O}(x^2) \right], \tag{B.4}
\end{aligned}$$

$$\begin{aligned}
\langle \zeta_{\mathbf{k}}(\eta) \zeta_{\mathbf{p}}(\eta) \rangle^{(e)} &= -\frac{32\tilde{\mathcal{C}}^2}{H^2} \delta^3(\mathbf{k} + \mathbf{p}) \int d\eta_1 \eta_1^{-1} \int d\eta_2 \eta_2^{-1} \int d^3\mathbf{p}_1 d^3\mathbf{p}_2 \delta^3(\mathbf{p}_1 + \mathbf{p}_2 - \mathbf{k}) \\
&\quad \times (\mathbf{k} \cdot \mathbf{p}_1)(\mathbf{k} \cdot \mathbf{p}_2) \text{Im} [\zeta_{\mathbf{k}}(\eta_1) \zeta_{\mathbf{k}}^*(\eta)] \text{Im} [\zeta_{\mathbf{k}}(\eta) \zeta_{\mathbf{k}}^*(\eta_2) \zeta_{\mathbf{p}_1}^{\prime}(\eta_1) \zeta_{\mathbf{p}_1}^*(\eta_2) \zeta_{\mathbf{p}_2}(\eta_1) \zeta_{\mathbf{p}_2}^{\prime}(\eta_2)] \\
&= \frac{2\pi^2}{k^3} \delta^3(\mathbf{k} + \mathbf{p}) \frac{16\tilde{\mathcal{C}}^2 |c_s|^2}{\pi H^2} A^6 \text{Im}[B]^2 e^{2k|c_s|\eta} (k|c_s|\eta - 1)^2 \\
&\quad \times \left[\frac{x^5}{150} (2 \log 2 - 1) - \frac{x^4}{240} (16 \log 2 - 15) - \frac{x^3}{360} (56 \log 2 - 17) + \mathcal{O}(x^2) \right].
\end{aligned} \tag{B.5}$$

Adding all these contributions yields the result quoted in the main text, Eq. (3.6).

C Other quartic scalar vertices

In the main text we considered, for simplicity, only a single quartic ζ vertex, i.e. ζ'^4 . The resulting one-loop correction to the scalar power spectrum was found to scale as x in the limit of large x , and is thus sub-dominant in comparison to the contributions from cubic vertices. In this Appendix we argue that the same scaling should appear in the results for the other two scalar vertices, i.e. $\zeta'^2(\partial\zeta)^2$ and $(\partial\zeta)^4$. We will carry out explicit calculations for the latter vertex, although it will become apparent that the same argument may be used for the other one in order to arrive at the same conclusion.

Consider then for concreteness the interaction Hamiltonian

$$H_{\zeta\zeta\zeta\zeta}^{(2)}(\eta) = \tilde{\mathcal{D}} \int d^3\mathbf{x} (\partial\zeta)^4, \quad \tilde{\mathcal{D}} \equiv \frac{M_{\text{Pl}}^2 \epsilon}{H^2 |c_s|^2} \mathcal{B}, \tag{C.1}$$

where \mathcal{B} is a dimensionless constant, expected to be $\mathcal{O}(1)$ in the EFT context. At leading order in x , i.e. upon maximizing the number of growing modes, in the loop integral, one has the diagram shown in Fig. 10, where we have separated the two types of permutations: one where both factors of $(\partial\zeta)^2$ share an external leg and an internal one, and one where one factor of $(\partial\zeta)^2$ is purely external and the other purely internal. The former permutation contributes a factor of $(\mathbf{k} \cdot \mathbf{p})^2$, where \mathbf{k} is the external momentum and \mathbf{p} is the internal one, while the latter contributes as $k^2 p^2$. Since $(\mathbf{k} \cdot \mathbf{p})^2 \leq k^2 p^2$, let us focus first only on the latter permutation for the purpose of estimating the size of the loop integral:

$$\tilde{\mathcal{I}}_2 = \int_{-x/k|c_s|}^{\eta} d\eta_1 \int_0^{-x/|c_s|\eta_1} dp k^2 p^2 \tilde{g}(p, \eta_1) e^{2p|c_s|\eta_1}, \tag{C.2}$$

where the blue factor is specific to the form of the $(\partial\zeta)^4$ vertex, as we just explained, and the function \tilde{g} encapsulates all other contributions (mode functions, coupling constants, etc.). We wish to compare (C.2) with the equivalent expression for the ζ'^4 vertex, see Eq. (3.3). Noting that

$$\zeta'_{p,\pm} = \pm \frac{p^2 |c_s|^2 \eta}{p |c_s| \eta - 1} \zeta_{p,\pm}, \tag{C.3}$$

it is straightforward to see that the dominant ζ'^4 loop integral is

$$\mathcal{I}_2 = \int_{-x/k|c_s|}^{\eta} d\eta_1 \int_0^{-x/|c_s|\eta_1} dp \frac{-p^4 |c_s|^8 \eta_1^4}{(p |c_s| \eta_1 - 1)^2 (k^2 |c_s|^2 \eta_1^2 - 1)} g(p, \eta_1) e^{2p|c_s|\eta_1}. \tag{C.4}$$

The functions $\tilde{g}(p, \eta_1)$ and $g(p, \eta_1)$ are the same up to coupling constants and order-one factors, so the point here is to compare the blue terms in Eqs. (C.2) and (C.4). One notes

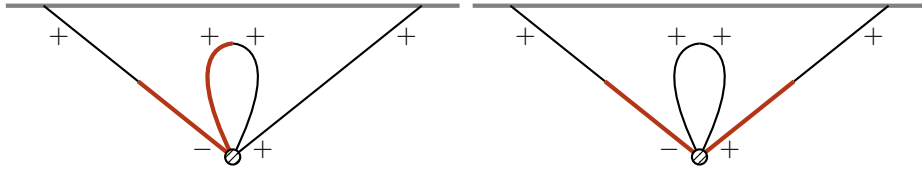


Figure 10. Two permutations of the one-loop diagram for the quartic vertex (C.1). Red lines indicate one pair $(\partial\zeta)^2$ out of the two in the vertex.

that both integrals are dominated by the region where $-p|c_s|\eta_1 \sim \mathcal{O}(1)$, and in fact the leading x behavior is obtained by setting $p \sim -1/|c_s|\eta_1$ and $\eta_1 \sim -x/k|c_s|$, for which both blue factors give the same scaling, namely $\propto x^{-2}$, and so both integrals will ultimately also scale in the same way, namely $\propto x$. The other vertex, $\zeta'^2(\partial\zeta)^2$, may be checked to produce the same result following an analogous argument.

As a final verification, we have performed the full calculation of the one-loop correction to the power spectrum from the $(\partial\zeta)^4$ vertex, with the result

$$\frac{k^3}{2\pi^2} \langle \zeta^2 \rangle'_{(\partial\zeta)^4} = \mathcal{P}_\zeta^2 \frac{\mathcal{B}}{|c_s|^4} e^{2k|c_s|\eta} (k|c_s|\eta - 1)^2 (9x + \mathcal{O}(x^0)) , \quad (\text{C.5})$$

confirming the $\propto x$ scaling of our quick estimate.

References

- [1] K. Kohri, D.H. Lyth and A. Melchiorri, *Black hole formation and slow-roll inflation*, *JCAP* **04** (2008) 038 [[0711.5006](#)].
- [2] M. Kawasaki, A. Kusenko, Y. Tada and T.T. Yanagida, *Primordial black holes as dark matter in supergravity inflation models*, *Phys. Rev. D* **94** (2016) 083523 [[1606.07631](#)].
- [3] J. Garcia-Bellido and E. Ruiz Morales, *Primordial black holes from single field models of inflation*, *Phys. Dark Univ.* **18** (2017) 47 [[1702.03901](#)].
- [4] K. Kannike, L. Marzola, M. Raidal and H. Veermäe, *Single Field Double Inflation and Primordial Black Holes*, *JCAP* **09** (2017) 020 [[1705.06225](#)].
- [5] C. Germani and T. Prokopec, *On primordial black holes from an inflection point*, *Phys. Dark Univ.* **18** (2017) 6 [[1706.04226](#)].
- [6] H. Motohashi and W. Hu, *Primordial Black Holes and Slow-Roll Violation*, *Phys. Rev. D* **96** (2017) 063503 [[1706.06784](#)].
- [7] H. Di and Y. Gong, *Primordial black holes and second order gravitational waves from ultra-slow-roll inflation*, *JCAP* **07** (2018) 007 [[1707.09578](#)].
- [8] G. Ballesteros and M. Taoso, *Primordial black hole dark matter from single field inflation*, *Phys. Rev. D* **97** (2018) 023501 [[1709.05565](#)].
- [9] M.P. Hertzberg and M. Yamada, *Primordial Black Holes from Polynomial Potentials in Single Field Inflation*, *Phys. Rev. D* **97** (2018) 083509 [[1712.09750](#)].
- [10] O. Özsoy, S. Parameswaran, G. Tasinato and I. Zavala, *Mechanisms for Primordial Black Hole Production in String Theory*, *JCAP* **07** (2018) 005 [[1803.07626](#)].
- [11] G. Ballesteros, J. Beltran Jimenez and M. Pieroni, *Black hole formation from a general quadratic action for inflationary primordial fluctuations*, *JCAP* **06** (2019) 016 [[1811.03065](#)].

- [12] R.-G. Cai, Z.-K. Guo, J. Liu, L. Liu and X.-Y. Yang, *Primordial black holes and gravitational waves from parametric amplification of curvature perturbations*, *JCAP* **06** (2020) 013 [[1912.10437](#)].
- [13] J. Lin, Q. Gao, Y. Gong, Y. Lu, C. Zhang and F. Zhang, *Primordial black holes and secondary gravitational waves from k and G inflation*, *Phys. Rev. D* **101** (2020) 103515 [[2001.05909](#)].
- [14] G. Ballesteros, J. Rey, M. Taoso and A. Urbano, *Primordial black holes as dark matter and gravitational waves from single-field polynomial inflation*, *JCAP* **07** (2020) 025 [[2001.08220](#)].
- [15] G.A. Palma, S. Sypsas and C. Zenteno, *Seeding primordial black holes in multifield inflation*, *Phys. Rev. Lett.* **125** (2020) 121301 [[2004.06106](#)].
- [16] J. Fumagalli, S. Renaux-Petel, J.W. Ronayne and L.T. Witkowski, *Turning in the landscape: A new mechanism for generating primordial black holes*, *Phys. Lett. B* **841** (2023) 137921 [[2004.08369](#)].
- [17] J. Fumagalli, S. Renaux-Petel and L.T. Witkowski, *Oscillations in the stochastic gravitational wave background from sharp features and particle production during inflation*, *JCAP* **08** (2021) 030 [[2012.02761](#)].
- [18] M. Braglia, X. Chen and D.K. Hazra, *Probing Primordial Features with the Stochastic Gravitational Wave Background*, *JCAP* **03** (2021) 005 [[2012.05821](#)].
- [19] J. Fumagalli, S. Renaux-Petel and L.T. Witkowski, *Resonant features in the stochastic gravitational wave background*, *JCAP* **08** (2021) 059 [[2105.06481](#)].
- [20] I. Dalianis, G.P. Kodaxis, I.D. Stamou, N. Tetradis and A. Tsigkas-Kouvelis, *Spectrum oscillations from features in the potential of single-field inflation*, *Phys. Rev. D* **104** (2021) 103510 [[2106.02467](#)].
- [21] J. Fumagalli, G.A. Palma, S. Renaux-Petel, S. Sypsas, L.T. Witkowski and C. Zenteno, *Primordial gravitational waves from excited states*, *JHEP* **03** (2022) 196 [[2111.14664](#)].
- [22] A. Karam, N. Koivunen, E. Tomberg, V. Vaskonen and H. Veermäe, *Anatomy of single-field inflationary models for primordial black holes*, *JCAP* **03** (2023) 013 [[2205.13540](#)].
- [23] K. Inomata, M. Braglia, X. Chen and S. Renaux-Petel, *Questions on calculation of primordial power spectrum with large spikes: the resonance model case*, *JCAP* **04** (2023) 011 [[2211.02586](#)].
- [24] J. Fumagalli, S. Bhattacharya, M. Peloso, S. Renaux-Petel and L.T. Witkowski, *One-loop infrared rescattering by enhanced scalar fluctuations during inflation*, *JCAP* **04** (2024) 029 [[2307.08358](#)].
- [25] A. Caravano, K. Inomata and S. Renaux-Petel, *Inflationary Butterfly Effect: Nonperturbative Dynamics from Small-Scale Features*, *Phys. Rev. Lett.* **133** (2024) 151001 [[2403.12811](#)].
- [26] A. Caravano, G. Franciolini and S. Renaux-Petel, *Ultraslow-roll inflation on the lattice: Backreaction and nonlinear effects*, *Phys. Rev. D* **111** (2025) 063518 [[2410.23942](#)].
- [27] V. Briaud, A. Karam, N. Koivunen, E. Tomberg, H. Veermäe and V. Vennin, *How deep is the dip and how tall are the wiggles in inflationary power spectra?*, [2501.14681](#).
- [28] S. Hawking, *Gravitationally collapsed objects of very low mass*, *Mon. Not. Roy. Astron. Soc.* **152** (1971) 75.
- [29] B.J. Carr and S.W. Hawking, *Black holes in the early Universe*, *Mon. Not. Roy. Astron. Soc.* **168** (1974) 399.
- [30] B.J. Carr, *The Primordial black hole mass spectrum*, *Astrophys. J.* **201** (1975) 1.
- [31] S. Mollerach, D. Harari and S. Matarrese, *CMB polarization from secondary vector and tensor modes*, *Phys. Rev. D* **69** (2004) 063002 [[astro-ph/0310711](#)].

- [32] K.N. Ananda, C. Clarkson and D. Wands, *The Cosmological gravitational wave background from primordial density perturbations*, *Phys. Rev. D* **75** (2007) 123518 [[gr-qc/0612013](#)].
- [33] D. Baumann, P.J. Steinhardt, K. Takahashi and K. Ichiki, *Gravitational Wave Spectrum Induced by Primordial Scalar Perturbations*, *Phys. Rev. D* **76** (2007) 084019 [[hep-th/0703290](#)].
- [34] K. Kohri and T. Terada, *Semianalytic calculation of gravitational wave spectrum nonlinearly induced from primordial curvature perturbations*, *Phys. Rev. D* **97** (2018) 123532 [[1804.08577](#)].
- [35] J.R. Espinosa, D. Racco and A. Riotto, *A Cosmological Signature of the SM Higgs Instability: Gravitational Waves*, *JCAP* **09** (2018) 012 [[1804.07732](#)].
- [36] S. Vagnozzi, *Inflationary interpretation of the stochastic gravitational wave background signal detected by pulsar timing array experiments*, *JHEAp* **39** (2023) 81 [[2306.16912](#)].
- [37] Y.-F. Cai, X.-C. He, X.-H. Ma, S.-F. Yan and G.-W. Yuan, *Limits on scalar-induced gravitational waves from the stochastic background by pulsar timing array observations*, *Sci. Bull.* **68** (2023) 2929 [[2306.17822](#)].
- [38] K. Inomata, K. Kohri and T. Terada, *Detected stochastic gravitational waves and subsolar-mass primordial black holes*, *Phys. Rev. D* **109** (2024) 063506 [[2306.17834](#)].
- [39] S. Wang, Z.-C. Zhao, J.-P. Li and Q.-H. Zhu, *Implications of pulsar timing array data for scalar-induced gravitational waves and primordial black holes: Primordial non-Gaussianity f_{NL} considered*, *Phys. Rev. Res.* **6** (2024) L012060 [[2307.00572](#)].
- [40] L. Liu, Z.-C. Chen and Q.-G. Huang, *Implications for the non-Gaussianity of curvature perturbation from pulsar timing arrays*, *Phys. Rev. D* **109** (2024) L061301 [[2307.01102](#)].
- [41] R. Ebadi, S. Kumar, A. McCune, H. Tai and L.-T. Wang, *Gravitational Waves from Stochastic Scalar Fluctuations*, [2307.01248](#).
- [42] D.G. Figueroa, M. Pieroni, A. Ricciardone and P. Simakachorn, *Cosmological Background Interpretation of Pulsar Timing Array Data*, *Phys. Rev. Lett.* **132** (2024) 171002 [[2307.02399](#)].
- [43] Z. Yi, Q. Gao, Y. Gong, Y. Wang and F. Zhang, *Scalar induced gravitational waves in light of Pulsar Timing Array data*, *Sci. China Phys. Mech. Astron.* **66** (2023) 120404 [[2307.02467](#)].
- [44] L. Liu, Z.-C. Chen and Q.-G. Huang, *Probing the equation of state of the early Universe with pulsar timing arrays*, *JCAP* **11** (2023) 071 [[2307.14911](#)].
- [45] X. Chen, *Primordial Non-Gaussianities from Inflation Models*, *Adv. Astron.* **2010** (2010) 638979 [[1002.1416](#)].
- [46] D. Wands, *Local non-Gaussianity from inflation*, *Class. Quant. Grav.* **27** (2010) 124002 [[1004.0818](#)].
- [47] Y. Wang, *Inflation, Cosmic Perturbations and Non-Gaussianities*, *Commun. Theor. Phys.* **62** (2014) 109 [[1303.1523](#)].
- [48] S. Renaux-Petel, *Primordial non-Gaussianities after Planck 2015: an introductory review*, *Comptes Rendus Physique* **16** (2015) 969 [[1508.06740](#)].
- [49] A. Achúcarro et al., *Inflation: Theory and Observations*, [2203.08128](#).
- [50] S. Renaux-Petel and K. Turzyński, *Geometrical Destabilization of Inflation*, *Phys. Rev. Lett.* **117** (2016) 141301 [[1510.01281](#)].
- [51] S. Cremonini, Z. Lalak and K. Turzynski, *Strongly Coupled Perturbations in Two-Field Inflationary Models*, *JCAP* **03** (2011) 016 [[1010.3021](#)].
- [52] A.R. Brown, *Hyperbolic Inflation*, *Phys. Rev. Lett.* **121** (2018) 251601 [[1705.03023](#)].

- [53] S. Renaux-Petel, K. Turzyński and V. Vennin, *Geometrical destabilization, premature end of inflation and Bayesian model selection*, *JCAP* **11** (2017) 006 [[1706.01835](#)].
- [54] S. Mizuno and S. Mukohyama, *Primordial perturbations from inflation with a hyperbolic field-space*, *Phys. Rev. D* **96** (2017) 103533 [[1707.05125](#)].
- [55] A. Achúcarro, R. Kallosh, A. Linde, D.-G. Wang and Y. Welling, *Universality of multi-field α -attractors*, *JCAP* **04** (2018) 028 [[1711.09478](#)].
- [56] P. Christodoulidis, D. Roest and E.I. Sfakianakis, *Angular inflation in multi-field α -attractors*, *JCAP* **11** (2019) 002 [[1803.09841](#)].
- [57] A. Linde, D.-G. Wang, Y. Welling, Y. Yamada and A. Achúcarro, *Hypernatural inflation*, *JCAP* **07** (2018) 035 [[1803.09911](#)].
- [58] S. Garcia-Saenz, S. Renaux-Petel and J. Ronayne, *Primordial fluctuations and non-Gaussianities in sidetracked inflation*, *JCAP* **07** (2018) 057 [[1804.11279](#)].
- [59] S. Garcia-Saenz and S. Renaux-Petel, *Flattened non-Gaussianities from the effective field theory of inflation with imaginary speed of sound*, *JCAP* **11** (2018) 005 [[1805.12563](#)].
- [60] A. Achúcarro and G.A. Palma, *The string swampland constraints require multi-field inflation*, *JCAP* **02** (2019) 041 [[1807.04390](#)].
- [61] P. Christodoulidis, D. Roest and E.I. Sfakianakis, *Attractors, Bifurcations and Curvature in Multi-field Inflation*, *JCAP* **08** (2020) 006 [[1903.03513](#)].
- [62] T. Bjorkmo and M.C.D. Marsh, *Hyperinflation generalised: from its attractor mechanism to its tension with the ‘swampland conditions’*, *JHEP* **04** (2019) 172 [[1901.08603](#)].
- [63] S. Garcia-Saenz, L. Pinol and S. Renaux-Petel, *Revisiting non-Gaussianity in multifield inflation with curved field space*, *JHEP* **01** (2020) 073 [[1907.10403](#)].
- [64] J. Fumagalli, S. Garcia-Saenz, L. Pinol, S. Renaux-Petel and J. Ronayne, *Hyper-Non-Gaussianities in Inflation with Strongly Nongeodesic Motion*, *Phys. Rev. Lett.* **123** (2019) 201302 [[1902.03221](#)].
- [65] T. Bjorkmo, *Rapid-Turn Inflationary Attractors*, *Phys. Rev. Lett.* **122** (2019) 251301 [[1902.10529](#)].
- [66] P. Christodoulidis, D. Roest and E.I. Sfakianakis, *Scaling attractors in multi-field inflation*, *JCAP* **12** (2019) 059 [[1903.06116](#)].
- [67] T. Bjorkmo, R.Z. Ferreira and M.C.D. Marsh, *Mild Non-Gaussianities under Perturbative Control from Rapid-Turn Inflation Models*, *JCAP* **12** (2019) 036 [[1908.11316](#)].
- [68] V. Aragam, S. Paban and R. Rosati, *Multi-field Inflation in High-Slope Potentials*, *JCAP* **04** (2020) 022 [[1905.07495](#)].
- [69] R. Bravo, G.A. Palma and S. Riquelme, *A Tip for Landscape Riders: Multi-Field Inflation Can Fulfill the Swampland Distance Conjecture*, *JCAP* **02** (2020) 004 [[1906.05772](#)].
- [70] D. Chakraborty, R. Chiovoloni, O. Loaiza-Brito, G. Niz and I. Zavala, *Fat inflatons, large turns and the η -problem*, *JCAP* **01** (2020) 020 [[1908.09797](#)].
- [71] R.Z. Ferreira, *Non-Gaussianities in models of inflation with large and negative entropic masses*, *JCAP* **08** (2020) 034 [[2003.13410](#)].
- [72] V. Aragam, S. Paban and R. Rosati, *The Multi-Field, Rapid-Turn Inflationary Solution*, *JHEP* **03** (2021) 009 [[2010.15933](#)].
- [73] V. Aragam, R. Chiovoloni, S. Paban, R. Rosati and I. Zavala, *Rapid-turn inflation in supergravity is rare and tachyonic*, *JCAP* **03** (2022) 002 [[2110.05516](#)].
- [74] S. Renaux-Petel, *Inflation with strongly non-geodesic motion: theoretical motivations and observational imprints*, *PoS EPS-HEP2021* (2022) 128 [[2111.00989](#)].

- [75] L. Anguelova and C.I. Lazaroiu, *Dynamical consistency conditions for rapid turn inflation*, *JCAP* **05** (2023) 020 [[2210.00031](#)].
- [76] P. Christodoulidis and J.-O. Gong, *Enhanced power spectra from multi-field inflation*, *JCAP* **08** (2024) 062 [[2311.04090](#)].
- [77] L. Anguelova, *On the consistency of rapid-turn inflation*, *Eur. Phys. J. C* **84** (2024) 941 [[2405.11595](#)].
- [78] R. Wolters, O. Iarygina and A. Achucarro, *Generalised conditions for rapid-turn inflation*, *JCAP* **07** (2024) 079 [[2405.11628](#)].
- [79] C. Gordon, D. Wands, B.A. Bassett and R. Maartens, *Adiabatic and entropy perturbations from inflation*, *Phys. Rev. D* **63** (2000) 023506 [[astro-ph/0009131](#)].
- [80] A.J. Tolley and M. Wyman, *The Gelaton Scenario: Equilateral non-Gaussianity from multi-field dynamics*, *Phys. Rev. D* **81** (2010) 043502 [[0910.1853](#)].
- [81] A. Achucarro, J.-O. Gong, S. Hardeman, G.A. Palma and S.P. Patil, *Features of heavy physics in the CMB power spectrum*, *JCAP* **01** (2011) 030 [[1010.3693](#)].
- [82] S. Cespedes, V. Atal and G.A. Palma, *On the importance of heavy fields during inflation*, *JCAP* **05** (2012) 008 [[1201.4848](#)].
- [83] A. Achucarro, V. Atal, S. Cespedes, J.-O. Gong, G.A. Palma and S.P. Patil, *Heavy fields, reduced speeds of sound and decoupling during inflation*, *Phys. Rev. D* **86** (2012) 121301 [[1205.0710](#)].
- [84] X. Chen, M.-x. Huang, S. Kachru and G. Shiu, *Observational signatures and non-Gaussianities of general single field inflation*, *JCAP* **01** (2007) 002 [[hep-th/0605045](#)].
- [85] C. Cheung, P. Creminelli, A.L. Fitzpatrick, J. Kaplan and L. Senatore, *The Effective Field Theory of Inflation*, *JHEP* **03** (2008) 014 [[0709.0293](#)].
- [86] R. Kallosh, A. Linde and D. Roest, *Superconformal Inflationary α -Attractors*, *JHEP* **11** (2013) 198 [[1311.0472](#)].
- [87] J.J.M. Carrasco, R. Kallosh, A. Linde and D. Roest, *Hyperbolic geometry of cosmological attractors*, *Phys. Rev. D* **92** (2015) 041301 [[1504.05557](#)].
- [88] L. Pinol, *Multifield inflation beyond $N_{\text{field}} = 2$: non-Gaussianities and single-field effective theory*, *JCAP* **04** (2021) 002 [[2011.05930](#)].
- [89] P. Christodoulidis and R. Rosati, *(Slow-)twisting inflationary attractors*, *JCAP* **09** (2023) 034 [[2210.14900](#)].
- [90] S. Weinberg, *Quantum contributions to cosmological correlations*, *Phys. Rev. D* **72** (2005) 043514 [[hep-th/0506236](#)].
- [91] K. Inomata, *Bound on induced gravitational waves during inflation era*, *Phys. Rev. D* **104** (2021) 123525 [[2109.06192](#)].
- [92] A. Ota, M. Sasaki and Y. Wang, *Scale-invariant enhancement of gravitational waves during inflation*, *Mod. Phys. Lett. A* **38** (2023) 2350063 [[2209.02272](#)].
- [93] A. Ota, M. Sasaki and Y. Wang, *One-loop tensor power spectrum from an excited scalar field during inflation*, *Phys. Rev. D* **108** (2023) 043542 [[2211.12766](#)].
- [94] J.-X. Feng, F. Zhang and X. Gao, *Scalar induced gravitational waves from Chern-Simons gravity during inflation era*, [2302.00950](#).
- [95] G. Ballesteros, S. C espedes and L. Santoni, *Large power spectrum and primordial black holes in the effective theory of inflation*, *JHEP* **01** (2022) 074 [[2109.00567](#)].
- [96] F. Piazza and F. Vernizzi, *Effective Field Theory of Cosmological Perturbations*, *Class. Quant. Grav.* **30** (2013) 214007 [[1307.4350](#)].

- [97] J. Garriga and V.F. Mukhanov, *Perturbations in k-inflation*, *Phys. Lett. B* **458** (1999) 219 [[hep-th/9904176](#)].
- [98] C. Armendariz-Picon, V.F. Mukhanov and P.J. Steinhardt, *A Dynamical solution to the problem of a small cosmological constant and late time cosmic acceleration*, *Phys. Rev. Lett.* **85** (2000) 4438 [[astro-ph/0004134](#)].
- [99] S. Renaux-Petel, *The Trispectrum as a Diagnostic of Primordial Orthogonal non-Gaussianities*, *JCAP* **07** (2013) 005 [[1302.6978](#)].
- [100] L. Senatore and M. Zaldarriaga, *On Loops in Inflation*, *JHEP* **12** (2010) 008 [[0912.2734](#)].
- [101] C. Cheung, A.L. Fitzpatrick, J. Kaplan and L. Senatore, *On the consistency relation of the 3-point function in single field inflation*, *JCAP* **02** (2008) 021 [[0709.0295](#)].
- [102] J.M. Maldacena, *Non-Gaussian features of primordial fluctuations in single field inflationary models*, *JHEP* **05** (2003) 013 [[astro-ph/0210603](#)].
- [103] S. Renaux-Petel, *On the redundancy of operators and the bispectrum in the most general second-order scalar-tensor theory*, *JCAP* **02** (2012) 020 [[1107.5020](#)].
- [104] C. Burrage, R.H. Ribeiro and D. Seery, *Large slow-roll corrections to the bispectrum of noncanonical inflation*, *JCAP* **07** (2011) 032 [[1103.4126](#)].
- [105] M. Braglia and L. Pinol, *No time to derive: unraveling total time derivatives in in-in perturbation theory*, *JHEP* **08** (2024) 068 [[2403.14558](#)].